Inclusive photoproduction of charmonia-bottomonia pairs

Marat Siddikov

Departamento de Física, Universidad Técnica Federico Santa María, y Centro Científico-Tecnológico de Valparaíso, Casilla 110-V, Valparaíso, Chile

(Received 31 January 2024; accepted 19 March 2024; published 1 May 2024)

In this article we analyze the inclusive photoproduction of heavy charmonia-bottomonia pairs in the color glass condensate framework and demonstrate that the cross section of the process is sensitive to dipole and quadrupole forward scattering amplitudes (2- and 4-point correlators of Wilson lines). Using the phenomenological parametrizations of these amplitudes, we estimate numerically the production cross sections in the kinematics of the forthcoming Electron Ion Collider and the ultraperipheral collisions at the LHC. We found that the contribution controlled by the quadrupole amplitude is dominant, and for this reason, the suggested channel can be used as a gateway for studies of this nonperturbative object.

DOI: 10.1103/PhysRevD.109.094001

I. INTRODUCTION

Due to their heavy masses and small sizes, quarkonia have been considered as important probes of the gluonic field of the target almost since their discovery [1,2]. The modern nonrelativistic quantum chromodynamics (NRQCD) framework allows one to evaluate systematically various perturbative corrections to processes which include quarkonia [3–13]. This framework allows one to get reasonable estimates for the cross sections, although at present it includes some uncertainties in nonperturbative long distance matrix elements (LDMEs) of quarkonia states [9–13], as well as apparent mismatch of the LDMEs of different quarkonia which challenge the expectations based on heavy quark mass limit [13–17]. Furthermore, even in the heavy quark mass limit the production of single quarkonia provides only limited information about the gluonic field. For this reason, since the early days of QCD theoretical efforts were dedicated to production mechanisms of multiple quarkonia in the final state [18–21], which could provide significantly more exhaustive information about the gluonic content of the target. Recent experiments at the LHC demonstrated a feasibility to study the production of quarkonia pairs experimentally.

In this paper we will focus on the associated production of charmonia and bottomonia, which have a very simple structure of the partonic amplitude. The theoretical studies of such processes (particularly, $J/\psi + \Upsilon$ hadroproduction) were initiated in [22–24] and attracted a lof of theoretical attention as possible probes of the gluonic field of the target. In the collinear and k_T factorization approach, such processes give a possibility to study the so-called double parton distribution functions (DPDFs), which encode the information about correlation of different constituents in the target. Recent experimental data [25,26] demonstrated that the double parton distributions might give significant contributions in this channel. However, due to a large number of different mechanisms in hadroproduction, these contributions have sophisticated structure, which complicates interpretation of experimental data in terms of partonic content of the target. At present the situation remains unclear: while inclusion of the DPDFs allows one to explain the difference between the data and predictions based on single-parton scattering, the value of the so-called effective cross-section $\sigma_{\rm eff}$ (parameter which controls the magnitude of the DPDFs) depends significantly on the channel used for its extraction [27–29]. In view of these difficulties of hadroproduction channel, the *photoproduction* of the same states can serve as a simpler alternative for testing our understanding of the contributing mechanisms. Previously, the studies of the double quarkonia photoproduction mostly focused on exclusive channels [30–39]. However, the inclusive production of such states also deserves interest as a potential gateway for studies of the gluonic distributions. Nowadays such processes may be studied in ultraperipheral pA collisions at the LHC, provided that the recoil nucleus is separated by a large rapidity gap from the other hadrons. The use of heavy ions allows one to boost significantly the flux of equivalent photons, and in this way facilitates measurement of tiny cross sections. In the future, such processes may also be studied in electron-proton collisions at the Electron Ion Collider (EIC) [40,41], the Large Hadron electron Collider (LHeC) [42], and the Future Circular Collider (FCC-he) [43–45].

In the kinematics of all the above-mentioned experiments, due to an enhanced role of multiparton distributions, which eventually lead to the onset of saturation effects, it is appropriate to analyze this process in the frameworks with built-in saturation. In what follows we will use for our studies a color glass condensate (CGC) framework [46–56], which naturally incorporates the saturation effects and provides a phenomenologically successful description of both hadron-hadron and lepton-hadron collisions [57–64]. The cross sections of physical processes in this framework are expressed in terms of the forward multipole scattering amplitudes (n-point correlators of Wilson lines), which have probabilistic interpretation and present important physical characteristics of the target. Technically, these correlators generalize the multigluon distribution functions used in a collinear and k_T factorization picture, providing correct asymptotic behavior in the high-energy limit.

The paper is structured as follows. In Sec. II we briefly describe the main components of the CGC framework and then present the theoretical results for the photoproduction of heavy quarkonia pairs in the CGC approach. In Sec. III we provide numerical estimates using the phenomenological parametrizations of dipole and quadrupole amplitudes. Finally, in Sec. IV we draw conclusions.

II. THEORETICAL FRAMEWORK

Nowadays, the photoproduction processes may be studied in electron-proton, proton-proton, and proton-nuclear collisions in ultraperipheral kinematics. The corresponding cross sections of these processes are related to the photoproduction cross section as

$$\frac{d\sigma_{ep\to eM_1M_2X}}{dQ^2dy_1d^2\boldsymbol{k}_1^\perp dy_2d^2\boldsymbol{k}_2^\perp}\approx\frac{\alpha_{\rm em}}{\pi Q^2}\left(1-y+\frac{y^2}{2}\right)\times\frac{d\sigma_T(\gamma+p\to M_1+M_2+X)}{dy_1d^2\boldsymbol{p}_1^\perp dy_2d^2\boldsymbol{p}_2^\perp}\bigg|_{\boldsymbol{p}_a^\perp\approx\boldsymbol{k}_a^\perp}, \tag{1}$$

$$\frac{d\sigma_{pA\to AM_1M_2X}}{dy_1d^2\boldsymbol{k}_1^\perp dy_2d^2\boldsymbol{k}_2^\perp}=\int dn_\gamma(\omega\equiv E_\gamma,\boldsymbol{q}_\perp)\times\frac{d\sigma_T(\gamma+p\to M_1+M_2+X)}{dy_1d^2\boldsymbol{p}_1^\perp dy_2d^2\boldsymbol{p}_2^\perp}\bigg|_{\boldsymbol{p}_a^\perp\approx\boldsymbol{k}_a^\perp-\boldsymbol{q}^\perp} \tag{2}$$

where in (1) we use standard deep inelastic scattering notations, in which y is the inelasticity (fraction of electron energy which passes to the photon), q and P are the 4-momenta of the photon and proton, and $(y_a,\boldsymbol{k}_a^\perp)$, with $a=1,2$, are the rapidities and transverse momenta of the produced quarkonia with respect to the electron-proton or hadron-hadron collision axis. The notation $d\sigma_T$ is used for the cross section of the photoproduction subprocess, induced by a transversely polarized photon. The expression $dn_\gamma(\omega\equiv E_\gamma,\boldsymbol{q}^\perp)$ in (2) is the spectral density of the flux of equivalent photons with energy E_γ and transverse momentum $\boldsymbol{q}^\perp$ with respect to the nucleus, which was found explicitly in [65]. The momenta $\boldsymbol{p}_a^\perp=\boldsymbol{k}_a^\perp-\boldsymbol{q}^\perp$ are the transverse parts of the quarkonia momenta with respect to the produced photon. Due to the nuclear form factor of the recoil nucleus, the spectral density $dn_\gamma(\omega,\boldsymbol{q}^\perp)$ is strongly suppressed for the transverse momenta $\boldsymbol{q}^\perp$ larger than the inverse nuclear radius R_A^{-1}, so the average values of $\boldsymbol{q}^\perp$ are quite small, $\langle\boldsymbol{q}_\perp^2\rangle\sim\langle Q^2\rangle\sim\langle R_A^2\rangle^{-1}\lesssim(0.2\ \mathrm{GeV}/A^{1/3})^2$, and the transverse momentum dependence of the cross sections in the left-hand side of (2) almost coincides with the $p_\perp$ dependence of the photoproduction cross section in the right-hand side, and for this reason from now on we will tacitly assume that $\boldsymbol{p}_a^\perp\approx\boldsymbol{k}_a^\perp$.

For further evaluations we need to fix the reference frame and write out explicit light-cone momenta decompositions of the participating hadrons. In what follows we will use notations p_1, p_2 for the 4-momenta of produced heavy quarkonia, and P for the momentum of the proton. We will work in the reference frame in which the light-cone expansion of these 4-vectors is given by

$$q=(q^+,0,\boldsymbol{0}_\perp),\qquad q^+=\sqrt{2}E_\gamma \tag{3}$$

$$P=\left(\frac{m_N^2}{2P^-},P^-,\boldsymbol{0}_\perp\right),\quad P^-=\frac{E_p+\sqrt{E_p^2-m_N^2}}{\sqrt{2}}\approx\sqrt{2}E_p, \tag{4}$$

$$p_a=\left(M_a^\perp e^{y_a},\frac{M_a^\perp e^{-y_a}}{2},\boldsymbol{p}_a^\perp\right),\quad a=1,2, \tag{5}$$

$$M_a^\perp\equiv\sqrt{M_a^2+(\boldsymbol{p}_a^\perp)^2}, \tag{6}$$

where m_N is the mass of the nucleon, and M_1, M_2 are the masses of the produced quarkonia. In what follows we will be mostly interested in the high-energy collider kinematics $q^+,P^-\gg\{Q,M_a,m_N\}$, when quarkonia are produced with relatively small transverse momenta. In this kinematics it is possible to use an eikonal picture and assume that the plus-component q^+ of the photon light-cone momentum is shared only between the produced quarkonia, namely

$$q^+\approx M_1^\perp e^{y_1}+M_2^\perp e^{y_2}. \tag{7}$$

The invariant energy W of the γp collision and the invariant mass M_{12} of the produced heavy quarkonia pair are given by

$$W^2\equiv s_{\gamma p}=(q+P)^2=-Q^2+m_N^2+2q\cdot P\approx-m_N^2+2P^-(M_1^\perp e^{y_1}+M_2^\perp e^{y_2}) \tag{8}$$

and

$$\mathcal{M}_{12}^2 = (p_1 + p_2)^2 = M_1^2 + M_2^2 + 2(M_1^\perp M_2^\perp \cosh \Delta y - \boldsymbol{p}_1^\perp \cdot \boldsymbol{p}_2^\perp) \tag{9}$$

respectively. The photoproduction cross section $d\sigma_T$, which appears in (1), (2), is the central quantity of interest for the present study and will be evaluated in the color glass condensate approach [46–56]. In the following Sec. II A we briefly remind the reader of the main assumptions of this theoretical framework, and in Sec. II B we present final theoretical results of the evaluation. To avoid possible soft factorization breaking final state interactions, in what follows we will tacitly assume that the produced quarkonia are kinematically well separated from each other, namely that the invariant relative velocity

$$v_{\rm rel} = \sqrt{1 - \frac{p_1^2 p_2^2}{(p_1 \cdot p_2)^2}} = \sqrt{1 - \frac{4M_1^2 M_2^2}{(\mathcal{M}_{12}^2 - M_1^2 - M_2^2)^2}} \tag{10}$$

is sufficiently large,

$$v_{\rm rel} \gtrsim v_{\rm rel}^{(\rm cutoff)} = 2\alpha_s(m_c) \approx 0.7, \tag{11}$$

or equivalently formulated in terms of the invariant mass of hadron pairs,

$$\mathcal{M}_{12}^2 \gtrsim (M_1 + M_2)^2 + 2M_1 M_2 \left(\frac{1}{\sqrt{1 - \left(v_{\rm rel}^{(\rm cutoff)}\right)^2}} - 1 \right). \tag{12}$$

A. High-energy scattering in CGC picture

For heavy quarkonia production, the heavy quark mass m_Q plays the role of the natural hard scale, which determines the interaction strength of heavy quarks with the gluonic field. In the heavy quark mass limit it is formally possible to develop a systematic expansion over the strong coupling $\alpha_s(m_Q) \ll 1$. However, such expansion might not be very reliable in the small-x limit, when the gluon fields are enhanced due to saturation effects and reach values $A_\mu^a \sim 1/\alpha_s$. The interaction of the partons with the ultrarelativistic target (shockwave) in this kinematics is characterized by nearly instantaneous color exchange, which can be described in the eikonal approximation. In this picture the interaction of a heavy quark with the target is described by a Wilson line $U(\boldsymbol{x}_\perp)$ [47–51,55,56]

$$U(\boldsymbol{x}_\perp) = P \exp\left(ig \int dx^- A_a^+(x^-, \boldsymbol{x}_\perp) t^a \right), \tag{13}$$

where $\boldsymbol{x}_\perp$ is the impact parameter of the parton, t_a are the ordinary color group generators of pQCD in fundamental representation, and $A_\mu^a(x) = -\frac{1}{\nabla_\perp^2}\rho_a(x^-, \boldsymbol{x})$ is the gluonic field in the target created by the color charge density ρ_a. According to classical CGC picture [47–49], for multiparton scattering processes each physical observable $\mathcal{O}$ should be averaged with a weight function $W[\rho]$ which describes the probability of a given charge distribution ρ inside the target, namely

$$\langle \mathcal{O} \rangle = \int \mathcal{D}\rho W[\rho] \mathcal{O}[\rho] \tag{14}$$

where from now on we will use angular brackets $\langle \ldots \rangle$ for such averaging. The analytic evaluation of the path integral $\mathcal{D}\rho$ is possible only for a few simple forms of $W[\rho]$ (e.g., for Gaussian). Fortunately, for many observables the averages $\langle \mathcal{O} \rangle$ may be expressed in terms of a limited set of universal (process-independent) amplitudes, such as dipole or quadrupole forward scattering amplitudes, thus avoiding explicit evaluation of the integral over all possible charge configurations.

For example, the amplitude of the heavy quark pair or (single) quarkonia production from a gluon may be described by the two diagrams shown in Fig. 1 (see for details [66–68]) and is given by

$$\mathcal{A}^a = -ig \int d^4 z \bar{u}(p_q, z) \gamma^\mu t^b \varepsilon_\mu^{ab}(k, z) v(p_{\bar{q}}, z), \tag{15}$$

where z represents the coordinate of the interaction point in the configuration space, and the corresponding parton fields are given by

$$\bar{u}(p_q, z) = \frac{1}{2}\left(\frac{p_q^+}{2\pi}\right) \int d^2\boldsymbol{x}_q e^{ip_q^+\left(z^- - \frac{(x_q - z)^2}{2z^+}\right) - i\boldsymbol{p}_q \cdot \boldsymbol{x}_q + \frac{iz^+}{2p_q^+}m^2} \times \left(\frac{i}{z^+}\right) \bar{u}_p \gamma^+ [U(\boldsymbol{x}_q)\theta(-z^+) + \theta(z^+)] \times \left(\gamma^- - \frac{\hat{\boldsymbol{x}}_q - \hat{\boldsymbol{z}}}{z^+} + \frac{m}{p_q^+}\right), \tag{16}$$

for the produced quarks,

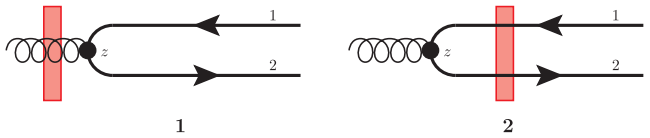

FIG. 1. Diagrams which describe the inclusive heavy quark pair production in the CGC picture in leading order over α_s. The subscript numbers 1, 2 enumerate the heavy quark lines in our convention. The subscript letter z is the coordinate of the interaction vertex in the configuration space. The red block represents the interaction with the target (shockwave).

$$v(p_{\bar q},z)=\frac{1}{2}\left(\frac{p^+_{\bar q}}{2\pi}\right)\int d^2\boldsymbol{x}_{\bar q}e^{ip^+_{\bar q}\left(z^- -\frac{(\boldsymbol{x}_{\bar q}-\boldsymbol{z})^2}{2z^+}\right)-i\boldsymbol{p}_{\bar q}\cdot\boldsymbol{x}_{\bar q}+\frac{iz^+}{2p^+_{\bar q}}m^2}\times\left(\frac{i}{z^+}\right)\left(\gamma^- -\frac{\hat{\boldsymbol{x}}_{\bar q}-\hat{\boldsymbol{z}}}{z^+}-\frac{m}{p^+_{\bar q}}\right)\times[U^\dagger(\boldsymbol{x}_{\bar q})\theta(-z^+)+\theta(z^+)]\gamma^+v_{p_{\bar q}} \tag{17}$$

for the produced antiquark, and

$$\varepsilon^{ba}_\mu(k,z)=\frac{k^+}{2\pi}\int d^2\boldsymbol{x}_g e^{-ik^+\left(z^- -\frac{(\boldsymbol{x}_g-\boldsymbol{z})^2}{2z^+}\right)+i\boldsymbol{k}\cdot\boldsymbol{x}_g}\times\left(\frac{-i}{z^+}\right)\left(g^\perp_{\mu\sigma}+\frac{x^\sigma_g-z^\sigma}{z^+}n^\mu_2\right)\times[\mathcal{U}^{ba}(\boldsymbol{x}_g)\theta(z^+)+\delta^{ab}\theta(-z^+)]\varepsilon^\sigma_\perp(\boldsymbol{k}) \tag{18}$$

for the initial-state gluon, where the vector n_2 in (18) is the unit light-cone vector pointing in the direction of the target momentum. The notation $\mathcal{U}^{ba}$ is used for the components of the matrix (13) in adjoint representation. The expressions in square brackets in (16)–(18) merely reflect that corresponding U-matrices should be taken into account only if the colored parton exists at the moment of interaction with the shockwave of the target. In the limit $U\to 1$ (no interaction) the amplitude (15) reduces to a mere perturbative spinor and gluon polarization vector. In what follows we will work in the mixed representation, describing the kinematics of each parton in terms of its light-cone momenta of the partons together with transverse coordinates in configuration space. Since in the eikonal approximation the interaction of any parton with the target is described by multiplicative factor $U(\boldsymbol{X}_p)$ in proper representation of the color group, evaluation of the amplitudes and cross sections becomes straightforward. For a simple process shown in (1), the amplitude of the process is described by the S-matrix element [55,56,60]

$$S_2(Y,\boldsymbol{x}_q,\boldsymbol{x}_{\bar q})=\frac{1}{N_c}\langle\mathrm{tr}(U(\boldsymbol{x}_q)U^\dagger(\boldsymbol{x}_{\bar q}))\rangle_Y, \tag{19}$$

where the notation Y is used for the dipole rapidity. The dipole scattering amplitude $N(x,\boldsymbol{r},\boldsymbol{b})$ can be related to $S_2(Y,\boldsymbol{x}_q,\boldsymbol{x}_{\bar q})$ as

$$N(x,\boldsymbol{r},\boldsymbol{b})=1-S_2(Y,\boldsymbol{x}_q,\boldsymbol{x}_{\bar q}), \tag{20}$$

where the variable $\boldsymbol{r}\equiv\boldsymbol{x}_q-\boldsymbol{x}_{\bar q}$ is the transverse size of the dipole, and $\boldsymbol{b}\equiv\alpha_q\boldsymbol{x}_q+\alpha_{\bar q}\boldsymbol{x}_{\bar q}$ is the transverse position of the dipole's center of mass. In complete analogy we may introduce the multipole scattering S-matrix elements (correlator of Wilson lines)

$$S_{2n}(Y,\boldsymbol{x}_1,\boldsymbol{\xi}_1,\ldots,\boldsymbol{x}_n,\boldsymbol{\xi}_n)=\frac{1}{N_c}\langle\mathrm{tr}(U(\boldsymbol{x}_1)U^\dagger(\boldsymbol{\xi}_1)\ldots U(\boldsymbol{x}_n)U^\dagger(\boldsymbol{\xi}_n))\rangle_Y, \tag{21}$$

which characterize the scattering amplitudes of a $2n$-particle ensemble of quarks. Each such correlator represents independent characteristics of the target and characterizes gluon distributions in the target.

1. Dilute scattering limit

If the saturation effects are not very large, the interaction of heavy quarks with the target can be described perturbatively, making a Taylor expansion of the Wilson line (13),

$$U(\boldsymbol{x}_\perp)\approx 1+ig\int dx^-A^+_a(x^-,\boldsymbol{x}_\perp)t^a+\frac{(ig)^2}{2!}P\int dx^-_1A^+_{a_1}(x^-_1,\boldsymbol{x}_{1\perp})\times\int dx^-_2A^+_{a_2}(x^-_2,\boldsymbol{x}_{2\perp})t^{a_1}t^{a_2}+\cdots. \tag{22}$$

The dipole scattering amplitude (20) in this limit may be expressed as

$$N(x,\boldsymbol{r},\boldsymbol{b})\approx\frac{1}{4N_c}\langle[\gamma_a(\boldsymbol{x}_Q)-\gamma_a(\boldsymbol{x}_{\bar Q})]^2\rangle+\mathcal{O}(\alpha_s), \tag{23}$$

where we defined γ_a as

$$\gamma_a(\boldsymbol{x})=g\int dx^-A^+_a(x^-,\boldsymbol{x})=g^2\int dx^-\frac{1}{\nabla^2_\perp}\rho_a(x^-,\boldsymbol{x}). \tag{24}$$

For further evaluation it is convenient to rewrite (24) in the form

$$\frac{1}{N_c}\langle\gamma_a(\boldsymbol{x}_1)\gamma_a(\boldsymbol{x}_2)\rangle=-2N(x,\boldsymbol{r}_{12},\boldsymbol{b}_{12})+\frac{\Gamma(\boldsymbol{x}_1)+\Gamma(\boldsymbol{x}_2)}{2N_c}, \tag{25}$$

where we introduced a shorthand notation $\Gamma(\boldsymbol{x})\equiv|\gamma_a(\boldsymbol{x})|^2$, and $\boldsymbol{r}_{12},\boldsymbol{b}_{12}$ are the transverse size and impact parameter of the color dipole. For certain processes which involve partonic ensembles with net zero color charge, the contributions $\sim\Gamma(\boldsymbol{x}_i)$ cancel, so the cross sections eventually can be represented entirely as a linear superposition of the dipole amplitudes $N(x,\boldsymbol{r},\boldsymbol{b})$. The multipole scattering amplitudes (21) in this limit may be rewritten as

$$S_{2n}(Y,\boldsymbol{x}_1,\boldsymbol{x}_2,\ldots,\boldsymbol{x}_{2n-1},\boldsymbol{x}_{2n})\approx\sum_{aijk\ell}c_{ijk\ell}(\gamma_a(\boldsymbol{x}_i)-\gamma_a(\boldsymbol{x}_j))(\gamma_a(\boldsymbol{x}_k)-\gamma_a(\boldsymbol{x}_\ell)), \tag{26}$$

where $c_{ijk\ell}$ are some numerical coefficients. Using the identities (25), it is possible to express (26) as a linear superposition of the forward color dipole amplitudes. However, at higher orders in $\alpha_s(m_Q)$ there are contributions

which include multiple products of $\gamma(x_k)$, and which cannot be reduced to a mere superposition of dipole amplitudes, demonstrating independence of the multipole contributions in a general case.

B. Inclusive photoproduction of meson pairs

The inclusive heavy quarkonia pair production in general may proceed via a number of different mechanisms, and for this reason presents a sophisticated problem. In what follows we will focus on the production of charmonia-bottomonia pairs with opposite C parity, in order to have vacuum quantum numbers in the t-channel. In the leading order of the perturbation theory at the amplitude level this process is described by a set of diagrams shown in Fig. 2. For comparison, the production of quarkonia pairs in a general case requires inclusion of additional Feynman diagrams shown in Fig. 3, or emission of additional hard gluons, leading to significantly more complicated expressions for the cross sections.

The evaluation of the diagrams shown in Fig. 2 is straightforward. The diagrams in the left and right rows might be related to each other by inversion of the quark line in the upper loop, and for this reason for quarkonia states with definite C parity give the same (up to a sign) contributions. According to NRQCD, the quarkonia formation can proceed both from color singlet and color octet $Q\bar{Q}$ pairs, so the total cross section may be represented as an incoherent sum

$$\frac{d\sigma}{d\Omega_h} = \frac{d\sigma^{(1)}}{d\Omega_h} + \frac{d\sigma^{(8)}}{d\Omega_h}, \tag{27}$$

where we introduced a shorthand notation $d\Omega_h = dy_1 d|p_1^\perp|^2 dy_2 d|p_2^\perp|^2 d\phi$ for the phase volume, ϕ is the azimuthal angle between the transverse momenta of the quarkonia, and $d\sigma^{(1)}, d\sigma^{(8)}$ stand respectively for the color singlet and octet contributions. The diagrams 1–4 lead to formation of $\bar{Q}Q$ pair (partons 3 and 4) in a color octet

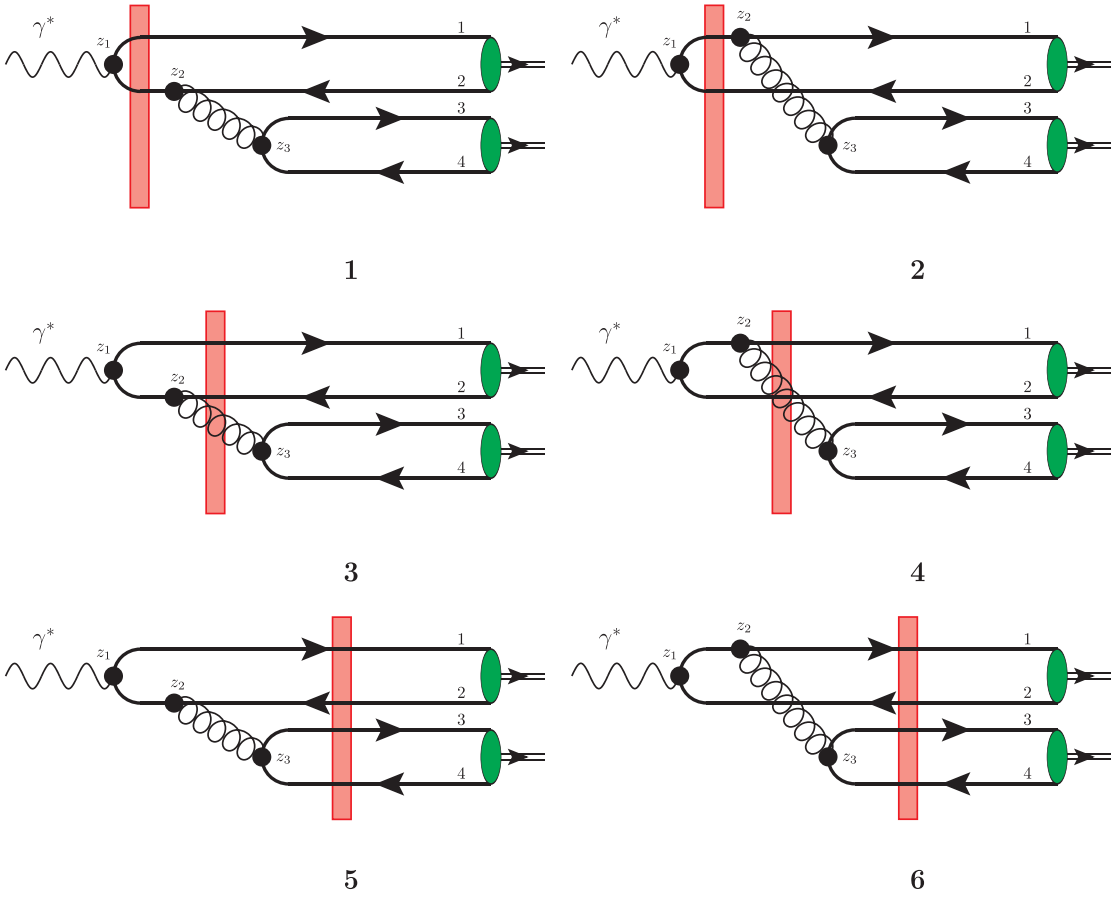

FIG. 2. Diagrams which describe the inclusive charmonia-bottomonia pairs production in the CGC picture in the leading order over α_s. The diagrams in the right column differ from diagrams in the left column just by inversion of the quark line in the upper loop (charge conjugation). The dominant color singlet contribution comes from the diagrams in the last row (diagrams 5 and 6 respectively). The subscript numbers 1–4 enumerate the heavy quark lines in our convention. The subscript letters $z_1 \ldots z_3$ stand for the coordinates of the interaction vertices in the configuration space. The red block represents the interaction with the target (shockwave).

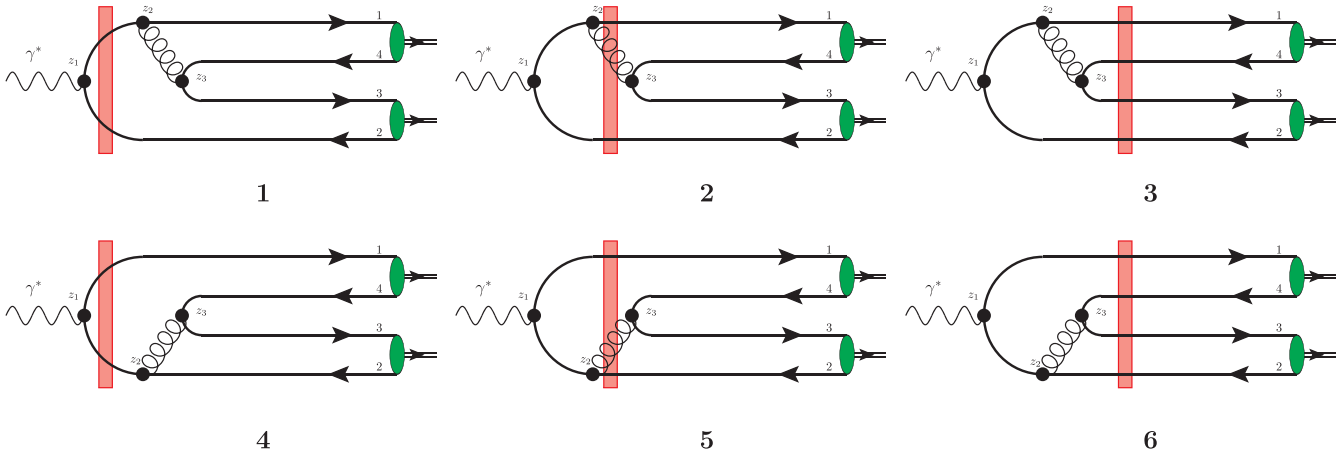

FIG. 3. Additional diagrams which in general should be taken into account for inclusive quarkonia pair production in the CGC picture in the leading order over α_s do not contribute to charmonia-bottomonia pairs. The subscript numbers 1–4 enumerate the heavy quark lines in our convention. The subscript letters $z_1 \ldots z_3$ stand for the coordinates of the interaction vertices in the configuration space. The red block represents the interaction with the target (shockwave).

state, whereas the remaining two diagrams lead to formation of both color singlet and color octet pairs. The evaluation of the color octet contribution, shown in diagrams 1–4 in the upper two rows may be interpreted as a production of the first quarkonium M_1 via $\gamma^* \to M_1 g$ subprocess, with subsequent fragmentation of the emitted hard gluon into the second quarkonium M_2. Indeed, we may observe that the gluon connecting quark lines of different heavy flavors is perturbative, and there is no instantaneous contributions to its propagator. For this reason, the contribution of diagrams 1–4 to the cross section may be rewritten as

$$\frac{d\sigma^{(8)}}{d\Omega_h} = \int \frac{dz}{z} D_{g\to M_2}(z) \frac{d\sigma_{\gamma^*\to M_1 g}(\boldsymbol{p}_{1M}, \boldsymbol{p}_g = \boldsymbol{p}_{2M}/z)}{d\Omega_h} \tag{28}$$

where $D_{g\to M_2}(z)$ is the fragmentation function of the gluon to the second quarkonium M_2 [69,70], and z is the fraction of the gluon momentum carried by the second quarkonium. In the leading order over $\alpha_s(m_Q)$, the fragmentation function is given by

$$D_{g\to M_2}(z) \approx \frac{\alpha_s}{m_c^3} \frac{\pi}{24} \left\langle \mathcal{O}^{M_2}\left({}^3S_1^{[8]}\right) \right\rangle \delta(z-1) \left(1 + \mathcal{O}\left(\frac{\Lambda_{\mathrm{QCD}}}{m_Q}\right)\right), \tag{29}$$

where $\langle \mathcal{O}^{M_2}({}^3S_1^{[8]}) \rangle$ is the corresponding color octet matrix element for the quarkonium M_2; however, at higher orders in $\alpha_s(m_Q)$, due to emission of soft gluons, the function $D_{g\to M_2}$ acquires nonzero finite width, and its peak shifts towards smaller $z < 1$ [70]. The evaluation of the cross-section $d\sigma_{\gamma^*\to M_1 g}$ may be found in [71] and largely repeats similar evaluation of the $\gamma^* \to \bar{Q}Qg$ subprocesses from [66,72]. The final result of this evaluation reads as [66,72]

$$\frac{d\sigma_{\gamma^*\to M_1 g}(\boldsymbol{p}_{1M}, \boldsymbol{p}_g)}{d\Omega_h^*} = \sum_{i,j=1}^{4} \frac{\mathrm{d}\hat{\sigma}_{i,j}^{\lambda}}{d\Omega_h^*} \tag{30}$$

$$\begin{aligned} &\frac{\mathrm{d}\hat{\sigma}_{i,j}^{\lambda}}{d\Omega_h^*} \\ &= \frac{1}{(q^+)^2} \frac{1}{(2\pi)^4} \frac{1}{8(1-x_g)} \\ &\times \int \mathrm{d}\Pi_i(\boldsymbol{p}, \boldsymbol{p}_g; \boldsymbol{r}, \boldsymbol{b}, z) \mathrm{d}\Pi_j^{\dagger}(\boldsymbol{p}, \boldsymbol{p}_g; \boldsymbol{r}', \boldsymbol{b}'_{12}, z') \\ &\times \Xi_{i,j}^{[c]}\left(\boldsymbol{b}_{12} + \frac{\boldsymbol{r}_{12}}{2}, \boldsymbol{b}_{12} - \frac{\boldsymbol{r}_{12}}{2}, z; \boldsymbol{b}'_{12} - \frac{\boldsymbol{r}'_{12}}{2}, \boldsymbol{b}'_{12} + \frac{\boldsymbol{r}'_{12}}{2}, z', Y\right) \\ &\times \Gamma_{i,j}^{\lambda}(\boldsymbol{p}, \boldsymbol{p}_g, Q; \boldsymbol{r}_{12}, \boldsymbol{b}_{12}, z, \boldsymbol{r}'_{12}, \boldsymbol{b}'_{12}, z'), \end{aligned} \tag{31}$$

where $\boldsymbol{b}_{12} = (\boldsymbol{x}_1 + \boldsymbol{x}_2)/2$ is the impact parameter of the quarkonium M_1, $\boldsymbol{r} = \boldsymbol{x}_1 - \boldsymbol{x}_2$ is the transverse distance between the quarks in the quarkonium, "primed" variables $\boldsymbol{b}', z', \boldsymbol{r}'$ correspond to similarly defined variables in the conjugate amplitude, and the corresponding differential measure of integration $\mathrm{d}\Pi_i(\ldots)$ is defined as

$$\mathrm{d}\Pi_i(\boldsymbol{p}, \boldsymbol{p}_g; \boldsymbol{r}, \boldsymbol{b}, z) = \mathrm{d}^2\boldsymbol{r} e^{-i\boldsymbol{p}_1\cdot\boldsymbol{b}} \mathrm{d}^2\boldsymbol{b} \begin{cases} \mathrm{d}^2\boldsymbol{z} e^{-i\boldsymbol{p}_g\cdot\boldsymbol{z}} & \text{if } i = 1, 3, \\ e^{-i\boldsymbol{p}_g\cdot(\boldsymbol{b}+\frac{\boldsymbol{r}}{2})} & \text{if } i = 2, \\ e^{-i\boldsymbol{p}_g\cdot(\boldsymbol{b}-\frac{\boldsymbol{r}}{2})} & \text{if } i = 4. \end{cases} \tag{32}$$

The explicit expressions for the matrices $\Xi_{i,j}^{[c]}$ and $\Gamma_{i,j}^{\lambda}$ may be found in [71] and will be omitted here for brevity. According to modern estimates [9,12,69,73–75], the color octet matrix elements $\mathcal{O}^M({}^3S_1^{[8]})$ are very small and constitute $\lesssim 10^{-2}$ of the color singlet matrix elements. For this

reason, a gluon fragmentation mechanism constitutes just a few percent correction and may be disregarded in the first approximation, especially in the kinematics of small transverse moments $p^\perp$ which we study in this paper.

In what follows we will focus on the contribution of the last two diagrams 5 and 6 in Fig. 2 which represent the dominant color singlet contributions. In evaluations we may use the fact that the final-state quarks are nearly on-shell, and in the eikonal picture the free quark propagator becomes diagonal in transverse coordinates in configuration space, namely

$$S_0(x-y) \approx \int \frac{dk^+ d^2\boldsymbol{k}_\perp}{(2\pi)^3}\frac{\gamma^+}{2k^+} e^{-ik\cdot(x-y)} \sim \delta(\boldsymbol{x}_\perp - \boldsymbol{y}_\perp) \quad (33)$$

(see details in [76]). The corresponding cross section in this limit may be rewritten as a convolution of wave functions and target-dependent multipole contributions, namely:

$$\begin{aligned}\frac{d\sigma}{d\Omega_h} = \int \left(\prod_{i=1}^4 d^2\boldsymbol{x}_i\right)\left(\prod_{i=1}^4 d^2\boldsymbol{x}'_i\right)\mathcal{N}(\boldsymbol{x}_1,\boldsymbol{x}_2,\boldsymbol{x}_3,\boldsymbol{x}_4;\boldsymbol{x}'_1,\boldsymbol{x}'_2,\boldsymbol{x}'_3,\boldsymbol{x}'_4)\\ \times \Psi^{\dagger h_1 h_2}_{M_1}\Psi^{\dagger h_3 h_4}_{M_2}\psi^{(\gamma)h_1h_2h_3h_4}_{\bar{Q}Q\bar{Q}Q}(\boldsymbol{x}_1;\boldsymbol{x}_2;\boldsymbol{x}_3;\boldsymbol{x}_4;q)e^{i(\boldsymbol{p}_1^\perp\cdot\tilde{\boldsymbol{b}}_{12}+\boldsymbol{p}_2^\perp\cdot\tilde{\boldsymbol{b}}_{34})}\\ \times (\Psi^{\dagger \mathfrak{h}_1 \mathfrak{h}_2}_{M_1}\Psi^{\dagger \mathfrak{h}_3 \mathfrak{h}_4}_{M_2}\psi^{(\gamma)\mathfrak{h}_1\mathfrak{h}_2\mathfrak{h}_3\mathfrak{h}_4}_{\bar{Q}Q\bar{Q}Q}(\boldsymbol{x}'_1;\boldsymbol{x}'_2;\boldsymbol{x}'_3;\boldsymbol{x}'_4;q)e^{i(\boldsymbol{p}_1^\perp\cdot\tilde{\boldsymbol{b}}'_{12}+\boldsymbol{p}_2^\perp\cdot\tilde{\boldsymbol{b}}'_{34})})^*,\end{aligned} \quad (34)$$

where h_i and $\mathfrak{h}_i$ are the helicities of heavy quarks in the amplitude and its conjugate (summation is implied), $\tilde{\boldsymbol{b}}_{ij} = \boldsymbol{b}_{ij} - \boldsymbol{r}_{ij}/2 \approx \boldsymbol{b}_{ij}$ is the impact parameter of the dipole made of partons i, and j [77–79] $\psi^{(\gamma)h_1h_2h_3h_4}_{\bar{Q}Q\bar{Q}Q}(\boldsymbol{x}_1;\boldsymbol{x}_2;\boldsymbol{x}_3;\boldsymbol{x}_4;q)$ is the wave function which describes the 4-quark $\bar{Q}Q\bar{Q}Q$ Fock state inside the quasireal photon (see details in Appendix A). We also use a shorthand notation $\Psi^{h_ih_j}_M$ for the conventional NRQCD projectors (in helicity basis) multiplied by the appropriate long distance matrix elements of the corresponding meson M. In the heavy quark mass limit the largest LDMEs are associated with the $^3S_1$, $^1S_0$, and $^1P_0$ states, for which the corresponding projectors are given by [5,6,8,80]

$$\Psi^{\dagger h_1 h_2}[^1S_0] = -\frac{1}{4N_c}\sqrt{\frac{\langle\mathcal{O}_M[^1S_0]\rangle}{m_Q}}\left[\gamma_5\left(\frac{\hat{P}_M}{2}+m_Q\right)\right]_{h_1h_2}, \quad (35)$$

$$\Psi^{\dagger h_1 h_2}[^3S_1] = -\frac{1}{4N_c}\sqrt{\frac{\langle\mathcal{O}_M[^1S_0]\rangle}{m_Q}}\left[\hat{\varepsilon}(S_z)\left(\frac{\hat{P}_M}{2}+m_Q\right)\right]_{h_1h_2}, \quad (36)$$

where P_M is the 4-momentum of the corresponding quarkonium, m_Q are the quarkonia masses, and $\langle\mathcal{O}_M\rangle$ are the corresponding long-distance matrix elements. We also introduced a shorthand notation,

$$\begin{aligned}\mathcal{N}(\boldsymbol{x}_1,\boldsymbol{x}_2,\boldsymbol{x}_3,\boldsymbol{x}_4;\boldsymbol{x}'_1,\boldsymbol{x}'_2,\boldsymbol{x}'_3,\boldsymbol{x}'_4) &= \langle \mathrm{tr}_c[t_a U(\boldsymbol{x}_1)U^\dagger(\boldsymbol{x}_2)]\mathrm{tr}_c[t_a U(\boldsymbol{x}_3)U^\dagger(\boldsymbol{x}_4)]\mathrm{tr}_c[t_b U(\boldsymbol{x}'_1)U^\dagger(\boldsymbol{x}'_2)]\mathrm{tr}_c[t_b U(\boldsymbol{x}'_3)U^\dagger(\boldsymbol{x}'_4)]\rangle\\ &= \frac{1}{4}\left\langle\left(\mathrm{tr}_c[U(\boldsymbol{x}_1)U^\dagger(\boldsymbol{x}_2)U(\boldsymbol{x}_3)U^\dagger(\boldsymbol{x}_4)] - \frac{1}{N_c}\mathrm{tr}_c[U(\boldsymbol{x}_1)U^\dagger(\boldsymbol{x}_2)]\mathrm{tr}_c[U(\boldsymbol{x}_3)U^\dagger(\boldsymbol{x}_4)]\right)\right.\\ &\quad\left.\times\left(\mathrm{tr}_c[U(\boldsymbol{x}'_1)U^\dagger(\boldsymbol{x}'_2)U(\boldsymbol{x}'_3)U^\dagger(\boldsymbol{x}'_4)] - \frac{1}{N_c}\mathrm{tr}_c[U(\boldsymbol{x}'_1)U^\dagger(\boldsymbol{x}'_2)]\mathrm{tr}_c[U(\boldsymbol{x}'_3)U^\dagger(\boldsymbol{x}'_4)]\right)\right\rangle\\ &= \frac{1}{4}\langle\mathrm{tr}_c[U(\boldsymbol{x}_1)U^\dagger(\boldsymbol{x}_2)U(\boldsymbol{x}_3)U^\dagger(\boldsymbol{x}_4)]\mathrm{tr}_c[U(\boldsymbol{x}'_1)U^\dagger(\boldsymbol{x}'_2)U(\boldsymbol{x}'_3)U^\dagger(\boldsymbol{x}'_4)]\rangle\\ &\quad - \frac{1}{4N_c}\langle\mathrm{tr}_c[U(\boldsymbol{x}_1)U^\dagger(\boldsymbol{x}_2)U(\boldsymbol{x}_3)U^\dagger(\boldsymbol{x}_4)]\mathrm{tr}_c[U(\boldsymbol{x}'_1)U^\dagger(\boldsymbol{x}'_2)]\mathrm{tr}_c[U(\boldsymbol{x}'_3)U^\dagger(\boldsymbol{x}'_4)]\rangle\\ &\quad - \frac{1}{4N_c}\langle\mathrm{tr}_c[U(\boldsymbol{x}_1)U^\dagger(\boldsymbol{x}_2)]\mathrm{tr}_c[U(\boldsymbol{x}_3)U^\dagger(\boldsymbol{x}_4)]\mathrm{tr}_c[U(\boldsymbol{x}'_1)U^\dagger(\boldsymbol{x}'_2)U(\boldsymbol{x}'_3)U^\dagger(\boldsymbol{x}'_4)]\rangle\\ &\quad + \left(\frac{1}{2N_c}\right)^2\langle\mathrm{tr}_c[U(\boldsymbol{x}_1)U^\dagger(\boldsymbol{x}_2)]\mathrm{tr}_c[U(\boldsymbol{x}_3)U^\dagger(\boldsymbol{x}_4)]\mathrm{tr}_c[U(\boldsymbol{x}'_1)U^\dagger(\boldsymbol{x}'_2)]\mathrm{tr}_c[U(\boldsymbol{x}'_3)U^\dagger(\boldsymbol{x}'_4)]\rangle,\end{aligned} \quad (37)$$

for the density matrix which describes interaction of the 4-quark ensemble with the target, with subsequent formation of two color singlet dipoles. The angular brackets $\langle\ldots\rangle$ denote averaging over the color sources, as defined in (14).

As we demonstrate in Appendix B, after convolution with color generators and color averaging, it is possible to rewrite (37) as

$$\mathcal{N}(\boldsymbol{x}_1,\boldsymbol{x}_2,\boldsymbol{x}_3,\boldsymbol{x}_4;\boldsymbol{x}_1',\boldsymbol{x}_2',\boldsymbol{x}_3',\boldsymbol{x}_4') = \frac{N_c^2}{4}\langle[S_4(\boldsymbol{x}_1,\boldsymbol{x}_2,\boldsymbol{x}_3,\boldsymbol{x}_4) - S_2(\boldsymbol{x}_1,\boldsymbol{x}_2)S_2(\boldsymbol{x}_3,\boldsymbol{x}_4)] \times [S_4(\boldsymbol{x}_1',\boldsymbol{x}_2',\boldsymbol{x}_3',\boldsymbol{x}_4') - S_2(\boldsymbol{x}_1',\boldsymbol{x}_2')S_2(\boldsymbol{x}_3',\boldsymbol{x}_4')]\rangle. \tag{38}$$

which includes only dipole and quadrupole correlators. In the usual large-N_c limit the averaging may be applied separately to different terms in the product in (38), so eventually the cross section probes the quadrupole and dipole forward scattering amplitudes. We need to mention that the combination of quadrupole and dipoles, $S_4(\boldsymbol{x}_1,\boldsymbol{x}_2,\boldsymbol{x}_3,\boldsymbol{x}_4) - S_2(\boldsymbol{x}_1,\boldsymbol{x}_2)S_2(\boldsymbol{x}_3,\boldsymbol{x}_4)$, which appears bilinearly in (38), also controls the dominant color singlet contribution in inclusive hadroproduction of single quarkonia [81]. In the latter channel the p_T dependence is predominanlty sensitive to the combination $\boldsymbol{x}_1+\boldsymbol{x}_2-\boldsymbol{x}_3-\boldsymbol{x}_4$ (difference of impact parameters of the produced quarkonia in the amplitude and its conjugate), whereas dependence on other combinations of transverse coordinates is integrated out in the heavy quark mass limit.[1] The double quarkonia production cross section (38) includes convolution with completely different dependence on coordinates, and for this reason provides an independent observable for study of the quadrupole contributions. In the special limit when the distance between any quark-antiquark pair vanishes, the quadrupole amplitude reduces to a dipole amplitude, and for this reason (38) cancels exactly. Due to this, the integral (34) remains finite despite of possible singular behavior of the wave function $\psi^{(\gamma)}_{\bar{Q}Q\bar{Q}Q}$ in this limit.

While the differential cross section (34) contains exhaustive information about the multipole elements of the target, due to smallness of the cross sections, experimentally it may be interesting to study the $\boldsymbol{p}_\perp$-integrated cross section, for which analytic integration over $\int d^2\boldsymbol{p}_1^\perp$ and $\int d^2\boldsymbol{p}_2^\perp$ yields

$$\begin{aligned}\frac{d\sigma}{dy_1dy_2} = 4(2\pi)^3\int d^2\boldsymbol{\xi}d^2\boldsymbol{\eta}\left(\prod_{i=1}^4 d^2\boldsymbol{x}_i\right) &\times \mathcal{N}(\boldsymbol{x}_1,\boldsymbol{x}_2,\boldsymbol{x}_3,\boldsymbol{x}_4;\boldsymbol{\xi},\boldsymbol{x}_1+\boldsymbol{x}_2-\boldsymbol{\xi},\boldsymbol{\eta},\boldsymbol{x}_3+\boldsymbol{x}_4-\boldsymbol{\eta}) \\ &\times [\Psi^{\dagger h_1h_2}_{M_1}\Psi^{\dagger h_3h_4}_{M_2}\psi^{(\gamma)h_1h_2h_3h_4}_{\bar{Q}Q\bar{Q}Q}(\boldsymbol{x}_1;\boldsymbol{x}_2;\boldsymbol{x}_3;\boldsymbol{x}_4;q)] \\ &\times (\Psi^{\dagger \bar{h}_1\bar{h}_2}_{M_1}\Psi^{\dagger \bar{h}_3\bar{h}_4}_{M_2}\psi^{(\gamma)\bar{h}_1\bar{h}_2\bar{h}_3\bar{h}_4}_{\bar{Q}Q\bar{Q}Q} \\ &\times (\boldsymbol{\xi};\boldsymbol{x}_1+\boldsymbol{x}_2-\boldsymbol{\xi};\boldsymbol{\eta};\boldsymbol{x}_3+\boldsymbol{x}_4-\boldsymbol{\eta};q))^*.\end{aligned} \tag{39}$$

[1]In our qualitative discussion of single quarkonia production we disregard additional phase factors $\sim e^{\pm i\boldsymbol{p}\cdot\boldsymbol{r}_{ij}}$ which take into account transverse boosts of the quarkonium wave function [77–79]. For quarkonia the typical dipole size $\boldsymbol{r}_{ij}$ is controlled by the heavy quark mass and becomes negligible in the heavy quark mass limit.

Finally, we would like to discuss briefly the evaluation of the diagrams shown in Fig. 3, which can contribute in the general case of quarkonia pair production. The evaluation largely follows the same procedure, however the interaction of the shock wave with heavy quarks at early stages (diagrams in the left and middle columns of Fig. 3) does not allow one to rewrite the cross section as a convolution of $\psi^{(\gamma)}_{\bar{Q}Q\bar{Q}Q}$ with a universal target-dependent structure even in eikonal approximation: due to the peculiar structure of the shockwave interaction with partons (16)–(18), there are no contributions with instantaneous virtual quarks and gluons which were taken into account in the evaluation of $\psi^{(\gamma)}_{\bar{Q}Q\bar{Q}Q}$. Since in the final state we register only the color singlet heavy quarkonia ($\approx$ take traces over the color indices of heavy quark lines, independently in the amplitude and its conjugate), the interaction with the target eventually can be expressed in terms of the dipole and quadrupole amplitudes (no sextupole and octupole contributions); however, the structure of such expressions will be different for the diagrams in each column of Fig. 3. A systematic evaluation for that case requires a dedicated study and will be presented elsewhere.

III. PHENOMENOLOGICAL ESTIMATES

A. Parametrization of the dipole and quadrupole amplitudes

The numerical estimates depend crucially on the choice of the parametrization of the dipole and quadrupole amplitudes. For the dipole amplitude N, we will use the phenomenological impact parameter b-dependent "bCGC" parametrization [78,82] which has correct asymptotic behavior in the small- and large-size dipole limits, and has been fitted to reproduce various phenomenological data with reasonable precision.

The quadrupole amplitude in general is an independent nonperturbative object, not related to a dipole amplitude. However, as was discussed in [83–85], in the limit of large number of colors $N_c \gg 1$, it is possible to relate various multipole and multitrace matrix elements, and essentially express them all in terms of the dipole amplitude N. For heavy charmonia in QCD, the use of the large-N_c limit is well justified, since the discarded $\sim\mathcal{O}(1/N_c)$ corrections parametrically are on par with strong coupling $\alpha_s(m_c)\sim 1/3$. The derivation of these identities is cumbersome and may be found in the above-mentioned references [83,84].

The possibility to express the amplitude in terms of the color singlet dipoles may be also understood from the *area enhancement argument* introduced in [86–88]: The interaction of the color singlet multipole (e.g., quadrupole) with the target grows as a function of its size due to color transparency; for this reason we expect that in the phase space integration, the dominant contribution should come from the configurations with well-separated partons in the transverse space. On the other hand, color group averaging suppresses correlators in which the distance between partons exceeding the color correlation length set by the saturation scale, namely $|\boldsymbol{x}_i-\boldsymbol{x}_j|\gtrsim Q_s^{-1}$. However, this suppression does not work for configurations in which all partons are grouped into small-size color singlet pairs, separated by large distances between pairs.[2] After the integration over phase space, it becomes clear that such multipair configurations are enhanced compared to true or "genuine" multipoles (quadrupoles). The enhancement factor is given by $\sim(S_\perp Q_s^2)^{n-1}$, where $S_\perp$ is the transverse area of the target, and $n\gtrsim 1$ is the number of color singlet pairs. According to modern phenomenological parametrizations, the typical values of saturation scale Q_s in the kinematics of interest are of order 1 GeV $\sim(0.2\text{ fm})^{-1}$; for this reason the enhancement factor $(S_\perp Q_s^2)$ might be numerically large even for the proton. For this reason, any multipoint correlator may be approximated as a sum of pairwise products [86–88]

$$\begin{aligned}&\langle U^\dagger(\boldsymbol{y}_1)^{a_1b_1}U(\boldsymbol{y}_2)^{a_2b_2}\ldots U^\dagger(\boldsymbol{y}_{2n-1})^{a_{2n-1}b_{2n-1}}U(\boldsymbol{y}_{2n})^{a_{2n}b_{2n}}\rangle\\&\approx\sum_{\sigma\in\Pi(\chi)}\prod_{\{\alpha,\beta\}\in\sigma}\langle U^\dagger(\boldsymbol{y}_\alpha)^{a_\alpha b_\alpha}U(\boldsymbol{y}_\beta)^{a_\beta b_\beta}\rangle,\end{aligned}\tag{40}$$

where $\chi=\{1,2,\ldots,2n\}$ and $\Pi(\chi)$ is the set of partitions of χ with disjoint pairs. The result (40) significantly simplifies evaluation of the diagrams with multipole contributions and allows one to apply Wick's theorem in order to introduce the glasma graph approach.

As was suggested in [83,84], the result (40) for the quadrupoles might be replaced with a more accurate expression which takes into account the effects of Jalilian-Marian, Iancu, McLerran, Weigert, Leonidov, and Kovner evolution, as well as has more accurate behavior in a few physically important limits. Explicitly, the amplitude $\overline{S_4}$ is given by

$$\begin{aligned}\overline{S_4}&\equiv\left\langle\frac{1}{N_c}\mathrm{tr}_c[U(\boldsymbol{x}_1)U^\dagger(\boldsymbol{x}_2)U(\boldsymbol{x}_3)U^\dagger(\boldsymbol{x}_4)]\right\rangle\\&\approx\frac{\Gamma_Y(\boldsymbol{x}_1,\boldsymbol{x}_2)+\Gamma_Y(\boldsymbol{x}_3,\boldsymbol{x}_4)-\Gamma_Y(\boldsymbol{x}_1,\boldsymbol{x}_3)-\Gamma_Y(\boldsymbol{x}_2,\boldsymbol{x}_4)}{\Gamma_Y(\boldsymbol{x}_1,\boldsymbol{x}_2)+\Gamma_Y(\boldsymbol{x}_3,\boldsymbol{x}_4)-\Gamma_Y(\boldsymbol{x}_1,\boldsymbol{x}_4)-\Gamma_Y(\boldsymbol{x}_2,\boldsymbol{x}_3)}\\&\quad\times\overline{S_2}(\boldsymbol{x}_1,\boldsymbol{x}_2)\overline{S_2}(\boldsymbol{x}_3,\boldsymbol{x}_4)\\&\quad+\frac{\Gamma_Y(\boldsymbol{x}_1,\boldsymbol{x}_4)+\Gamma_Y(\boldsymbol{x}_2,\boldsymbol{x}_3)-\Gamma_Y(\boldsymbol{x}_1,\boldsymbol{x}_3)-\Gamma_Y(\boldsymbol{x}_2,\boldsymbol{x}_4)}{\Gamma_Y(\boldsymbol{x}_1,\boldsymbol{x}_4)+\Gamma_Y(\boldsymbol{x}_2,\boldsymbol{x}_3)-\Gamma_Y(\boldsymbol{x}_1,\boldsymbol{x}_2)-\Gamma_Y(\boldsymbol{x}_3,\boldsymbol{x}_4)}\\&\quad\times\overline{S_2}(\boldsymbol{x}_1,\boldsymbol{x}_4)\overline{S_2}(\boldsymbol{x}_2,\boldsymbol{x}_3)\end{aligned}\tag{41}$$

where the function $\Gamma_Y(\boldsymbol{x}_i,\boldsymbol{x}_j)$ is defined as

$$\Gamma_Y(\boldsymbol{x}_i,\boldsymbol{x}_j)=-\ln\left(\overline{S_2}(\boldsymbol{x}_i,\boldsymbol{x}_j)\right)=-\ln\left(1-N(x,\boldsymbol{r}_{ij},\boldsymbol{b}_{ij})\right).\tag{42}$$

The expression (41) includes denominators vanishing at the hypersurface

$$\Gamma_Y(\boldsymbol{x}_1,\boldsymbol{x}_2)+\Gamma_Y(\boldsymbol{x}_3,\boldsymbol{x}_4)=\Gamma_Y(\boldsymbol{x}_1,\boldsymbol{x}_4)+\Gamma_Y(\boldsymbol{x}_2,\boldsymbol{x}_3);\tag{43}$$

however, the function $\bar{S}_4$ remains finite when approaching this hypersurface, with limiting value given by

$$\begin{aligned}\overline{S_4}|_{(43)}&\approx\overline{S_2}(\boldsymbol{x}_1,\boldsymbol{x}_2)\overline{S_2}(\boldsymbol{x}_3,\boldsymbol{x}_4)\\&\quad\times\left(1+\ln\left(\frac{\overline{S_2}(\boldsymbol{x}_1,\boldsymbol{x}_2)\overline{S_2}(\boldsymbol{x}_3,\boldsymbol{x}_4)}{\overline{S_2}(\boldsymbol{x}_1,\boldsymbol{x}_3)\overline{S_2}(\boldsymbol{x}_2,\boldsymbol{x}_4)}\right)\right).\end{aligned}\tag{44}$$

The combination $\overline{S_4}(\boldsymbol{x}_1,\boldsymbol{x}_2,\boldsymbol{x}_3,\boldsymbol{x}_4)-\overline{S_2}(\boldsymbol{x}_1,\boldsymbol{x}_2)\overline{S_2}(\boldsymbol{x}_3,\boldsymbol{x}_4)$ which appears in (38) may be rewritten as

$$\begin{aligned}&\overline{S_4}(\boldsymbol{x}_1,\boldsymbol{x}_2,\boldsymbol{x}_3,\boldsymbol{x}_4)-\overline{S_2}(\boldsymbol{x}_1,\boldsymbol{x}_2)\overline{S_2}(\boldsymbol{x}_3,\boldsymbol{x}_4)\\&\approx\frac{\Gamma_Y(\boldsymbol{x}_1,\boldsymbol{x}_4)+\Gamma_Y(\boldsymbol{x}_2,\boldsymbol{x}_3)-\Gamma_Y(\boldsymbol{x}_1,\boldsymbol{x}_3)-\Gamma_Y(\boldsymbol{x}_2,\boldsymbol{x}_4)}{\Gamma_Y(\boldsymbol{x}_1,\boldsymbol{x}_4)+\Gamma_Y(\boldsymbol{x}_2,\boldsymbol{x}_3)-\Gamma_Y(\boldsymbol{x}_1,\boldsymbol{x}_2)-\Gamma_Y(\boldsymbol{x}_3,\boldsymbol{x}_4)}\\&\quad\times[\overline{S_2}(\boldsymbol{x}_1,\boldsymbol{x}_2)\overline{S_2}(\boldsymbol{x}_3,\boldsymbol{x}_4)+\overline{S_2}(\boldsymbol{x}_1,\boldsymbol{x}_4)\overline{S_2}(\boldsymbol{x}_2,\boldsymbol{x}_3)].\end{aligned}\tag{45}$$

In the dilute limit, the expression for $\overline{S_4}$ simplifies as [83,84]

$$\begin{aligned}\overline{S_4}&\equiv\left\langle\frac{1}{N_c}\mathrm{tr}_c[U(\boldsymbol{x}_1)U^\dagger(\boldsymbol{x}_2)U(\boldsymbol{x}_3)U^\dagger(\boldsymbol{x}_4)]\right\rangle\\&\approx 1-N(x,\boldsymbol{r}_{12},\boldsymbol{b}_{12})-N(x,\boldsymbol{r}_{34},\boldsymbol{b}_{34})-N(x,\boldsymbol{r}_{23},\boldsymbol{b}_{23})\\&\quad-N(x,\boldsymbol{r}_{14},\boldsymbol{b}_{14})+N(x,\boldsymbol{r}_{13},\boldsymbol{b}_{13})+N(x,\boldsymbol{r}_{24},\boldsymbol{b}_{24}).\end{aligned}\tag{46}$$

Substituting this result into the amplitude (37), it is possible to show that the nonzero contributions show up only when we take into account the nonlinear $\sim\mathcal{O}(N^2)$ terms in expansion and reads as

[2]Formally in our expansion we should take into account all groups of matrices which include color singlet irreducible representation in expansion of direct product, for example color triplets $\langle U(\boldsymbol{x}_1)U(\boldsymbol{x}_2)U(\boldsymbol{x}_3)\rangle$ for $N_c=3$. However, from the area enhancement argument it is clear that the dominant contribution comes from the configurations with maximal number of disjoint blocks, which corresponds to pairwise products $U^\dagger(\boldsymbol{x}_1)U(\boldsymbol{x}_2)$.

$$\mathcal{N}(\boldsymbol{x}_1,\boldsymbol{x}_2,\boldsymbol{x}_3,\boldsymbol{x}_4;\boldsymbol{x}'_1,\boldsymbol{x}'_2,\boldsymbol{x}'_3,\boldsymbol{x}'_4)$$
$$\approx \frac{N_c^2}{4}[N(x,\boldsymbol{r}_{13},\boldsymbol{b}_{13})+N(x,\boldsymbol{r}_{24},\boldsymbol{b}_{24})-N(x,\boldsymbol{r}_{23},\boldsymbol{b}_{23})$$
$$-N(x,\boldsymbol{r}_{14},\boldsymbol{b}_{14})][N(x,\boldsymbol{r}'_{13},\boldsymbol{b}'_{13})+N(x,\boldsymbol{r}'_{24},\boldsymbol{b}'_{24})$$
$$-N(x,\boldsymbol{r}'_{23},\boldsymbol{b}'_{23})-N(x,\boldsymbol{r}'_{14},\boldsymbol{b}'_{14})]. \quad (47)$$

The expressions in the second and the third lines of (47) may be rewritten using identity

$$N(x,\boldsymbol{r}_{13},\boldsymbol{b}_{13})+N(x,\boldsymbol{r}_{24},\boldsymbol{b}_{24})$$
$$-N(x,\boldsymbol{r}_{23},\boldsymbol{b}_{23})-N(x,\boldsymbol{r}_{14},\boldsymbol{b}_{14})$$
$$\approx [N(x,\boldsymbol{r}_{13},\boldsymbol{b}_{13})-N(x,\boldsymbol{r}_{23},\boldsymbol{b}_{23})]$$
$$-[N(x,\boldsymbol{r}_{14},\boldsymbol{b}_{14})-N(x,\boldsymbol{r}_{24},\boldsymbol{b}_{24})] \quad (48)$$

which clearly shows that (47) vanishes when any of the dipole sizes $\boldsymbol{r}_{12},\boldsymbol{r}_{34},\boldsymbol{r}'_{12},\boldsymbol{r}'_{34}$ goes to zero. Indeed, as was discussed in the previous section, in this limit the quadrupole amplitude reduces to a dipole amplitude and exactly cancels in (38). In the small-r domain it is expected that the dipole amplitude N should have an asymptotic behavior

$$N(x,\boldsymbol{r},\boldsymbol{b}) \approx (Q_s^2(x,\boldsymbol{b})r^2)^{\gamma}, \quad (49)$$

where Q_s is the saturation scale, and $\gamma \lesssim 1$ is some numerical coefficient. For $\gamma \approx 1$ (e.g., "GBW" and "bSat" parametrizaitons [89]) it is possible to simplify drastically (47) and rewrite it as

$$\mathcal{N}^{(\gamma=1)}(\boldsymbol{x}_1,\boldsymbol{x}_2,\boldsymbol{x}_3,\boldsymbol{x}_4;\boldsymbol{x}'_1,\boldsymbol{x}'_2,\boldsymbol{x}'_3,\boldsymbol{x}'_4)$$
$$\approx \frac{N_c^2 Q_s^4(x)}{2}(\boldsymbol{r}_{12}\cdot\boldsymbol{r}_{34})(\boldsymbol{r}'_{12}\cdot\boldsymbol{r}'_{34}), \quad (50)$$

which demonstrates the dependence of the scattering amplitude $\mathcal{N}$ on sizes of individual dipoles in a heavy quark mass limit. For $\gamma \neq 1$ a simple form (50) is not valid. However the antisymmetry of (47) with respect to permutations $\boldsymbol{r}_1 \leftrightarrow \boldsymbol{r}_2, \boldsymbol{r}_3 \leftrightarrow \boldsymbol{r}_4$ indicates that the amplitude (47) should have a pronounced sensitivity to a relative orientation of vectors $(\boldsymbol{r}_{12},\boldsymbol{r}_{34})$ and $(\boldsymbol{r}'_{12},\boldsymbol{r}'_{34})$.

B. Numerical estimates for fully differential cross sections

For the sake of definiteness, we will focus on the production of the $J/\psi+\eta_b$ and $\Upsilon(1S)+\eta_c$ production, which are expected to have the largest cross section among all of the charmonia-bottomonia pairs. We disregard the color octet channels in view of the smallness of the color octet LDMEs. For the dominant color singlet LDMEs we will use the values [9,74,75]

$$\left\langle \mathcal{O}^{J/\psi}\left({}^3S_1^{[1]}\right)\right\rangle \approx 3\langle \mathcal{O}^{\eta_c}({}^1S_0^{[1]})\rangle \approx 1.16\ \text{GeV}^3, \quad (51)$$

$$\left\langle \mathcal{O}^{\Upsilon(1S)}\left({}^3S_1^{[1]}\right)\right\rangle \approx 3\langle \mathcal{O}^{\eta_b}({}^1S_0^{[1]})\rangle \approx 8.39\ \text{GeV}^3, \quad (52)$$

where the LDMEs of pseudoscalar mesons are fixed using the relations valid in the heavy quark mass limit [3]. As expected from potential models [90–93], these LDMEs approximately scale with a heavy quark mass as $\sim(\alpha_s(m_Q)m_Q)^3$.

In Fig. 4 we illustrate the transverse momentum dependence of the cross section for different quarkonia states. Following the tradition, for the ultraperipheral pA collisions at the LHC, the cross sections in what follows are given on a per nucleon basis (divided by atomic mass number A respectively). A significant increase of the per-nucleon cross section in pA collisions at the LHC can be explained by the factor $\sim Z^2$ in the photon flux, where Z is the atomic number of the projectile nucleus. The significant difference of $J/\psi\eta_b$ and $\Upsilon(1S)\eta_c$ cross sections might be understood in the dilute limit: in this case the pseudoscalar quarkonium can originate only from the secondary (lower) quark loop in Fig. 2. The virtuality of the gluon which connects the two loops is largely controlled by the mass of this pseudoscalar quarkonium, thus yielding a relative suppression factor

$$\frac{d\sigma_{\gamma p\to J/\psi\eta_b}}{d\sigma_{\gamma p\to\Upsilon(1S)\eta_c}} \sim \left(\frac{M_{\eta_c}}{M_{\eta_b}}\right)^4 \sim 10^{-2}. \quad (53)$$

In Fig. 5 we study the dependence of the cross sections on the azimuthal angle ϕ between the transverse momenta of the two quarkonia states. In order to make meaningful comparison of the cross sections, which differ by orders of magnitude, we plotted the normalized ratio of the cross sections,

$$R(\phi) = \frac{d\sigma(\ldots,\phi)/d\Omega_h}{d\sigma(\ldots,\phi_{\max})/d\Omega_h}, \quad (54)$$

where $\phi_{\max}$ is the angle which maximizes the numerators of (54). Since the quarkonia (dipole) sizes are small in the heavy quark mass limit, the dependence on transverse momenta in the small-p_T kinematics is largely sensitive to the dependence on the (Fourier conjugate) impact parameters $\boldsymbol{b}_{12}=(\boldsymbol{x}_1+\boldsymbol{x}_2)/2$ and $\boldsymbol{b}_{34}=(\boldsymbol{x}_3+\boldsymbol{x}_4)/2$ in the implemented quadrupole amplitude. For the parametrization (41), the dependence on angle φ between the centers of mass of the dipoles, $\boldsymbol{b}_{12}$ and $\boldsymbol{b}_{34}$, is largely controlled by prefactor

$$\sim\Gamma_Y(\boldsymbol{x}_1,\boldsymbol{x}_4)+\Gamma_Y(\boldsymbol{x}_2,\boldsymbol{x}_3)-\Gamma_Y(\boldsymbol{x}_1,\boldsymbol{x}_3)-\Gamma_Y(\boldsymbol{x}_2,\boldsymbol{x}_4)$$
$$\approx\Gamma_Y\left(\boldsymbol{b}_{12}-\boldsymbol{b}_{34}+\frac{\boldsymbol{r}_{12}+\boldsymbol{r}_{34}}{2}\right)+\Gamma_Y\left(\boldsymbol{b}_{12}-\boldsymbol{b}_{34}-\frac{\boldsymbol{r}_{12}+\boldsymbol{r}_{34}}{2}\right)$$
$$-\Gamma_Y\left(\boldsymbol{b}_{12}-\boldsymbol{b}_{34}+\frac{\boldsymbol{r}_{12}-\boldsymbol{r}_{34}}{2}\right)-\Gamma_Y\left(\boldsymbol{b}_{12}-\boldsymbol{b}_{34}-\frac{\boldsymbol{r}_{12}-\boldsymbol{r}_{34}}{2}\right), \quad (55)$$

where we introduced variables $\boldsymbol{r}_{ij}=\boldsymbol{x}_i-\boldsymbol{x}_j$ for the distance between pairs of the heavy quarks. In the heavy quark mass limit, the dominant contribution comes from the region $r_{12}, r_{34} \ll b_{12}, b_{34}$. For the angle $\varphi \approx 0$ (collinearly directed impact parameters), the factor (55) is suppressed at $\boldsymbol{b}_{12} \approx \boldsymbol{b}_{34}$:

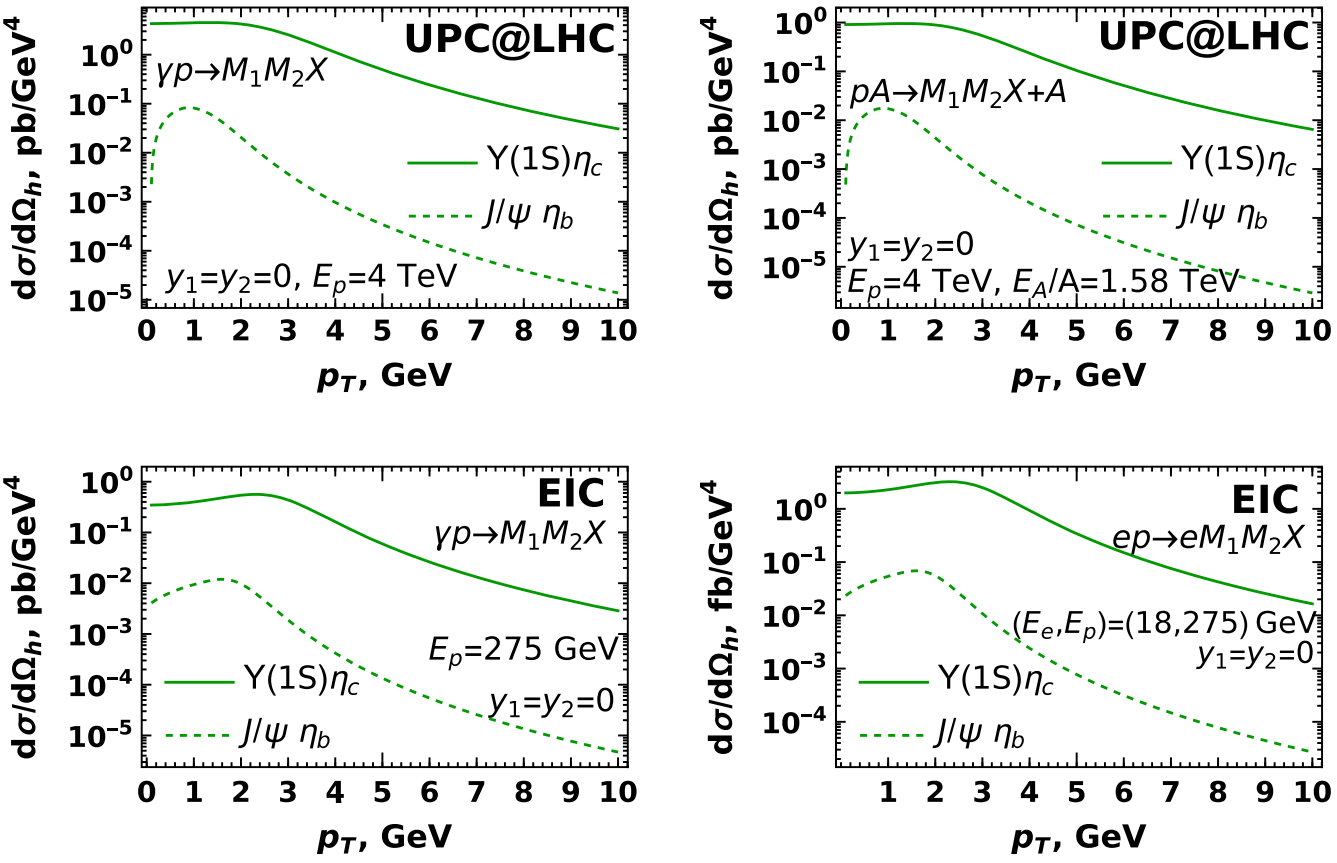

FIG. 4. The cross sections of inclusive production of different quarkonia pairs with opposite C parities. For the sake of definiteness we considered that both quarkonia are produced with the same absolute value of the transverse momenta $p_1^\perp = p_2^\perp = p_T$. Upper and lower rows correspond to kinematics of ultraperipheral collisions and the Electron-Ion Collider, respectively. The left column corresponds to cross sections of the photon-proton subprocess, the right column includes predictions for the cross section of the full process. For ultraperipheral kinematics at the LHC we consider collisions of protons with lead ($^{208}_{82}$Pb) ions, and the cross sections are given per nucleon. For the EIC we considered the electron-proton collisions only; for heavy nuclei these results should be understood as cross sections per nucleon. For the sake of definiteness we considered production at central rapidities ($y_1 = y_2 = 0$) in the lab frame. The shape of the p_T dependence has a very mild dependence on rapidity and azimuthal angle ϕ between the produced quarkonia.

physically this corresponds to a tiny quadrupole passing at some distance from the nucleus. The cross section increases homogeneously as a function of ϕ, which merely reflects growth of the quadrupole moment of the four-quark ensemble. The predicted pronounced ϕ dependence suggests that predominantly the production occurs in the back-to-back kinematics, akin to exclusive photoproduction of the same pairs [37]. In order to demonstrate that the expected ϕ dependence is due to the implemented parametrization of the quadrupole amplitude, in the second row of Fig. 5 we compare predictions obtained with the parametrization (41) and a trivial parametrization

$$S_4(\boldsymbol{x}_1, \boldsymbol{x}_2, \boldsymbol{x}_3, \boldsymbol{x}_4) = 1, \tag{56}$$

which corresponds to a free noninteracting quadrupole. For the latter parametrization, integration of the quadrupole terms in (34) yields δ functions $\sim\delta(\boldsymbol{p}_1^\perp), \delta(\boldsymbol{p}_2^\perp)$, so for nonzero momenta $\boldsymbol{p}_1^\perp, \boldsymbol{p}_2^\perp$ the quadrupole contribution effectively drops out. As we can see from the last row in Fig. 5, the ϕ dependence in this case is negligibly small: it exists due to a mild dependence on orientation of the two dipoles $\boldsymbol{r}_{12}, \boldsymbol{r}_{34}$ in the wave function $\psi^{(\gamma)}_{\bar{Q}Q\bar{Q}Q}$. This finding corroborates that the predicted ϕ dependence is due to the chosen parametrization of the quadrupole amplitude.

In order to understand how the quadrupoles affect the *magnitude* of the cross section, in Fig. 6 we plotted the ratio

$$\mathcal{R}(\phi) = \frac{d\sigma^{(41)}/d\Omega_h}{d\sigma^{(56)}/d\Omega_h}, \tag{57}$$

in which the numerator and denominator were found using parametrizations (41) and (56), respectively. Since the parametrization (56) does not include quadrupole interaction with the target, the deviations of the ratio (57) from unity can be used to assess the relative importance of the quadrupole scattering implemented in parametrization (41).

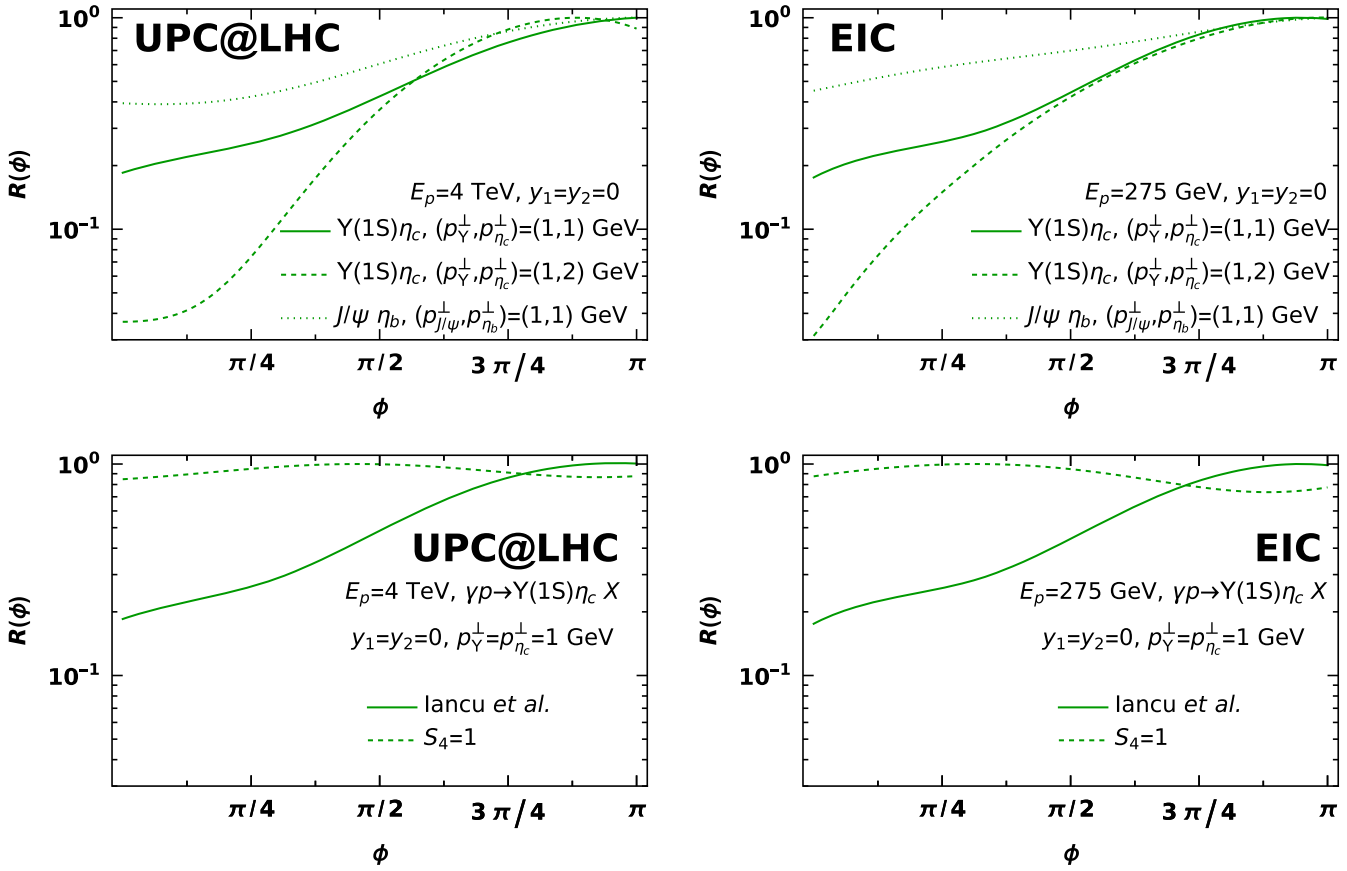

FIG. 5. Upper row: dependence of the normalized ratio $R(\phi)$, defined in (54), on the angle ϕ (azimuthal angle between transverse momenta of quarkonia). Left plot corresponds to the kinematics of ultraperipheral collisions at the LHC; right plot is for the kinematics of the Electron-Ion Collider. The cross section has almost the same angular dependence for all rapidities and transverse momenta p_T (see the text for more detailed explanation). Lower row: comparison of angular dependence found with parametrization (41) (curve with label "Iancu *et al.*") and a trivial parametrization (56).

From Fig. 6 we may conclude that in parametrization (41) the quadrupole scattering gives the dominant contribution.

Finally, in the Figs. 7 and 8 we show the dependence on quarkonia rapidities in the LHC and EIC kinematics. The growth of the cross section as a function of average rapidity $Y = (y_1 + y_2)/2$ merely repeats the rapidity dependence (growth) of the dipole scattering amplitude, which contributes directly and indirectly via parametrization of the quadrupole amplitude. In the second row of Figs. 7 and 8 we show the dependence of the cross section on the rapidity difference Δy between the two heavy mesons. For simplicity we made plots for the quarkonia having opposite rapidities in the lab frame, $y_1 = -y_2 = \Delta y/2$. The configurations with large rapidity difference correspond to highly asymmetric sharing of the photon momentum between the quarks, for which the wave function $\psi^{(\gamma)}_{\bar{Q}Q\bar{Q}Q}$ is strongly suppressed. For this reason, the quarkonia are predominantly produced with close rapidities. Since the variable Δy may be related to the invariant mass of the heavy quarkonia pairs (9), this behavior implies suppression of the cross section for large invariant masses of charmonia-bottomonia pairs.

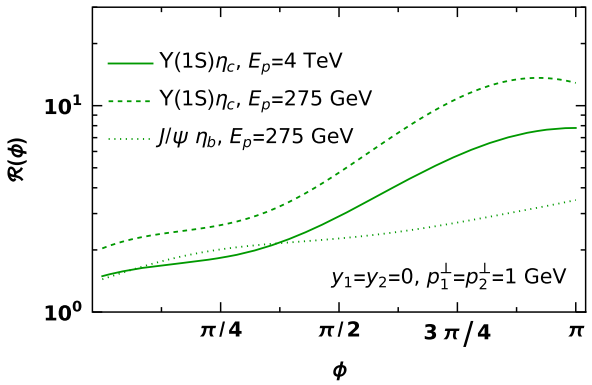

FIG. 6. The ratio of the cross sections (57) found with different parametrizations of the quadrupole amplitude. The deviation of this ratio from unity demonstrates the dominance of the quadrupole contribution in the parametrization (41).

C. Numerical estimates for integrated cross sections

Up to now we considered the fully differential cross sections, which present ideal probes for theoretical studies.

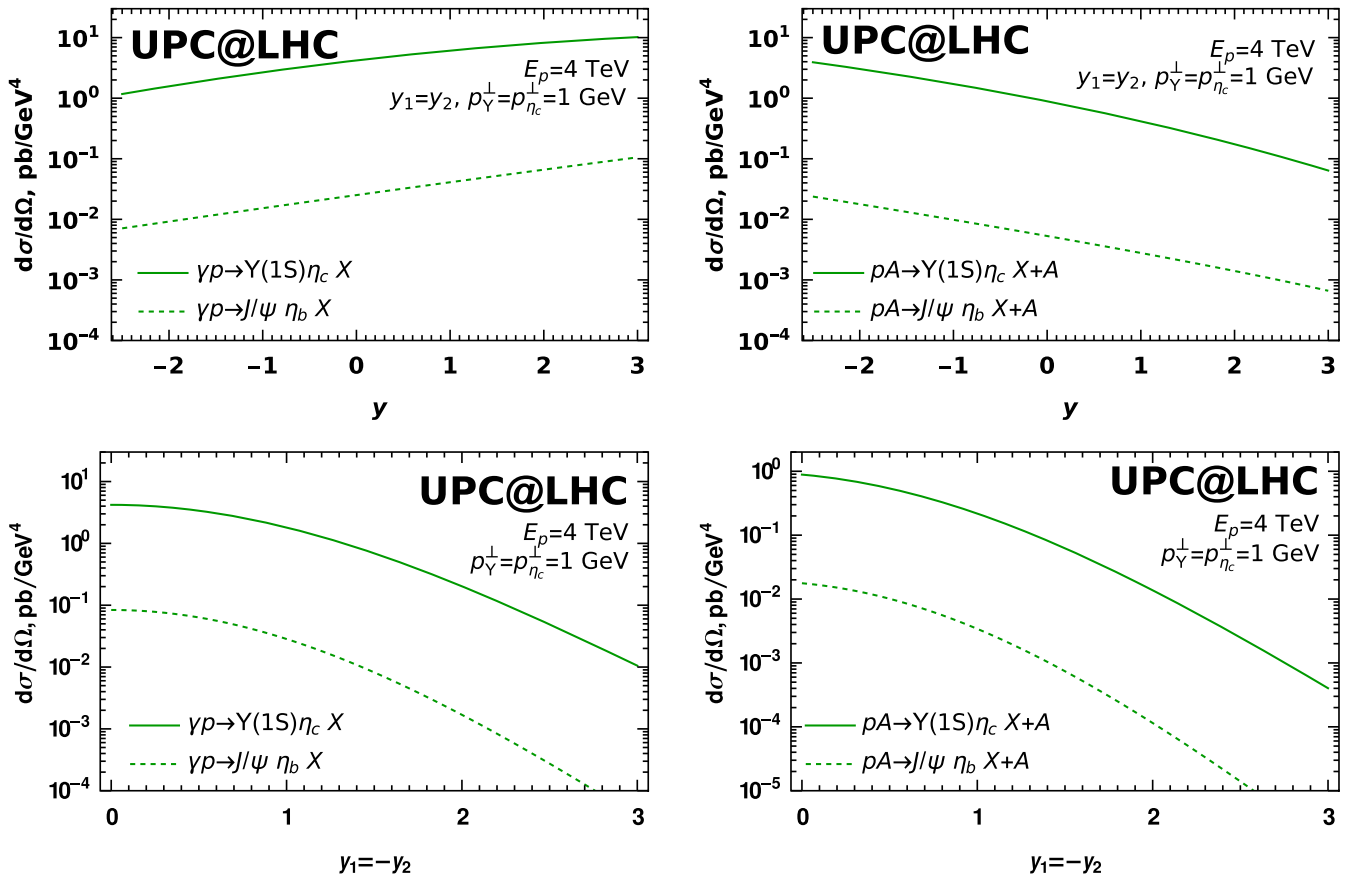

FIG. 7. Rapidity dependence of the cross section in the kinematics of the ultraperipheral collisions at the LHC. Plots in the upper row correspond to a configuration with equal rapidities of the produced quarkonia, $y_1 = y_2$, whereas the lower row corresponds to rapidities which differ by a sign in lab frame, $y_1 = -y_2$. In both rows the left plot corresponds to the cross section of the *photoproduction* subprocess, and the right column shows predictions for the cross section of the full process $pA \to A + M_1 M_2 X$, assuming proton-lead collisions, as defined in (2).

However, experimentally, it can be challenging to access them directly because of insufficient statistics, and for this reason in this section we will provide predictions for the yields integrated over some or all kinematic variables. A comparison of theoretical predictions and experimental data for such observables requires due care, since integration over kinematic variables commingles contributions from different domains, and potentially can include contributions from the regions where the theoretical approach might be not valid. The CGC framework is well justified in the small-x_B region,

$$x_B \approx \frac{\mathcal{M}_{12}^2}{W^2} \lesssim 10^{-2}, \tag{58}$$

though sometimes CGC might give a reasonable description up to much higher values of $x_B \sim 0.1$. In order to avoid an additional uncertainty due to extrapolations, we will focus on the small-x_B domain and assume that the cross section vanishes if the constraint (58) is not satisfied. In LHC kinematics the constraint (58) is fulfilled practically for all rapidities and almost does not affect the integrated observables. However, for EIC kinematics the constraint (58) limits the possible range of rapidities y_1, y_2 of the produced quarkonia and suppresses the expected yields by up to an order of magnitude. The total ("fiducial") cross sections in the EIC and LHC kinematics are given in Table I. A significant enhancement of the *per nucleon* cross section in pA collisions compared to pp can be explained by the factor $\sim Z^2$ in the photon flux, where Z is the atomic number of the projectile nucleus. In the same table we also provide predictions for the total number of quarkonia pair photoproduction events and the production rate

$$N_{\rm tot} = \sigma_{\rm tot} \times \mathcal{L}_{\rm int}, \qquad \frac{dN_{\rm tot}}{dt} = \sigma_{\rm tot} \times \mathcal{L}, \tag{59}$$

using the values of the instantaneous luminosity $\mathcal{L}$ and integrated luminosity $\mathcal{L}_{\rm int} = \int dt \mathcal{L}$ from [40,41,94]. The expected number of events in ep collisions at EIC and in pA collisions at LHC are comparable, despite a significant difference of the cross sections, because the luminosity at the EIC will exceed by several orders of magnitude the

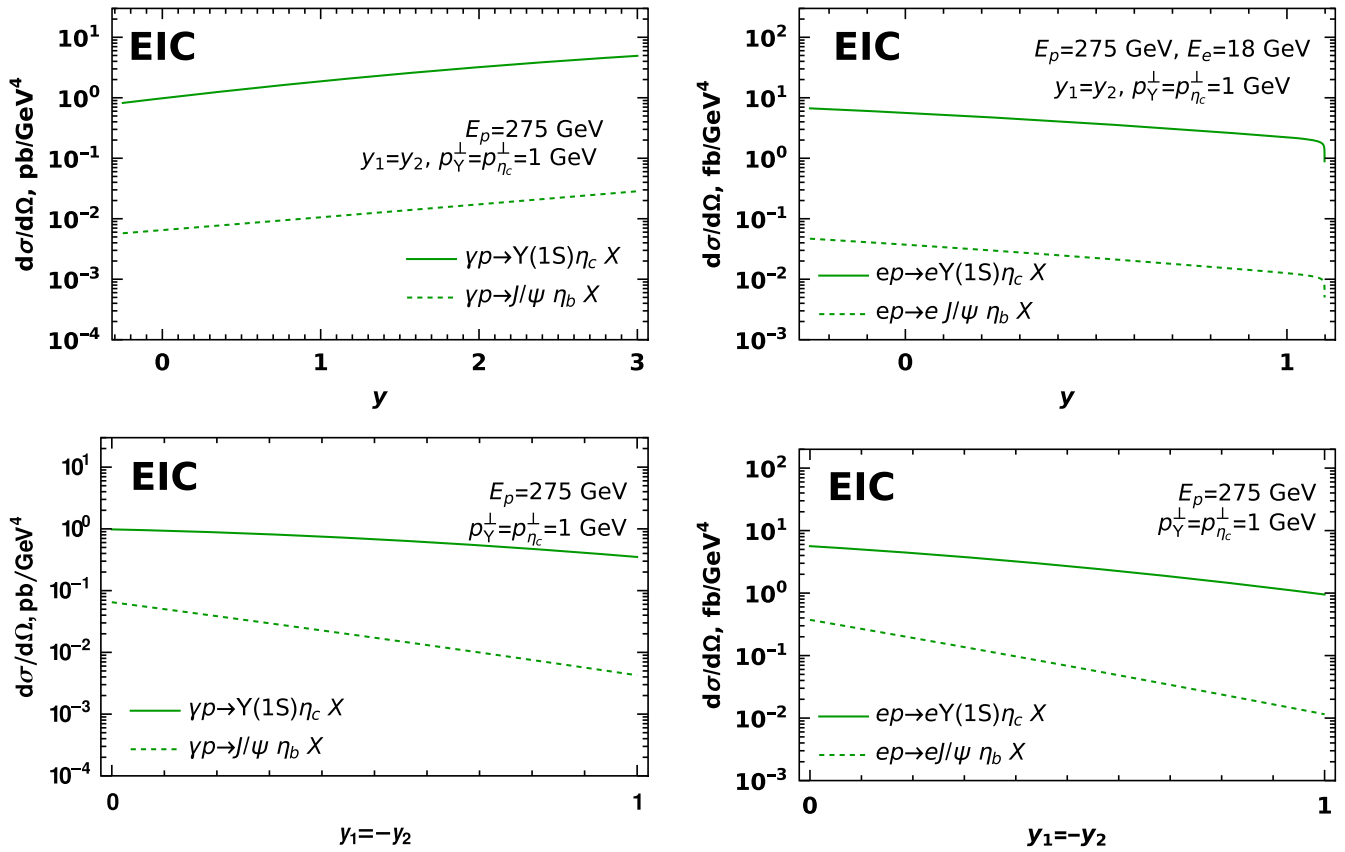

FIG. 8. Rapidity dependence of the cross section in the kinematics of the future Electron-Ion Collider. The left column corresponds to the cross section of the *photoproduction* subprocess, and the right column shows predictions for the cross section of the full electroproduction process $eA \to eAM_1M_2X$. Due to the heavy mass of the final state, the CGC approach is not applicable for $y \lesssim -1$, and for $y \gtrsim 1$ the flux of the equivalent photons is suppressed due to leptonic factor (energy of the emitted virtual photon approaches from below the energy of the electron).

TABLE I. The total (fiducial) cross section for several channels and estimates for the produced/collected number of events at the EIC and LHC. $\sigma_{\rm tot}$ is the total (fiducial) cross sections [with constraint (58) imposed during phase space integration]; $N_{\rm tot}$ and $dN_{\rm tot}/dt$ are the total number of produced pairs and the production rates, respectively. N_d and dN_d/dt are the expected total number of the collected events and counting rates defined in (60). The values of instantaneous luminosity $\mathcal{L}$ and integrated luminosity $\mathcal{L}_{\rm int} = \int dt \mathcal{L}_{\rm int}$ are taken from [40,41,94]. For pA collisions the cross sections and luminosities are given per nucleon pair, for proton-lead ($^{208}_{82}$Pb) collisions.

Process	$\sqrt{s}$	$\mathcal{L}$, cm^{-2} s^{-1}	$\mathcal{L}_{\rm int}$	$\sigma_{\rm tot}$	$N_{\rm tot}$	$dN_{\rm tot}/dt$	N_d	dN_d/dt
			ep collisions at EIC					
$ep \to e\Upsilon\eta_c X$	141 GeV	10^{34}	100 fb^{-1}	3 pb	3×10^5	2.6×10^3/day	198	1.69/day
$ep \to eJ/\psi\eta_b X$				9.9 fb	990	8.5/day	⋯	⋯
			Ultraperipheral pp collisions at LHC					
$pp \to p\Upsilon\eta_c X$	14 TeV	10^{34}	100 fb^{-1}	0.13 nb	1.3×10^7	1.1×10^5/day	8.5×10^3	73/day
$pp \to pJ/\psi\eta_b X$				0.17 pb	1.7×10^4	1.6×10^2/day	⋯	⋯
			Ultraperipheral pA collisions at LHC					
$ep \to e\Upsilon\eta_c X$	5.02 TeV	10^{30}	100 pb^{-1}	2.1 nb	2.1×10^5	1.8×10^2/day	1.3×10^2	0.12/day
	8.16 TeV			3.7 nb	3.7×10^5	3.2×10^2/day	2.4×10^2	0.2/day
$ep \to eJ/\psi\eta_b X$	5.02 TeV			3.6 pb	3.6×10^2	0.3/day	⋯	⋯
	8.16 TeV			4.9 pb	4.9×10^2	0.4/day	⋯	⋯

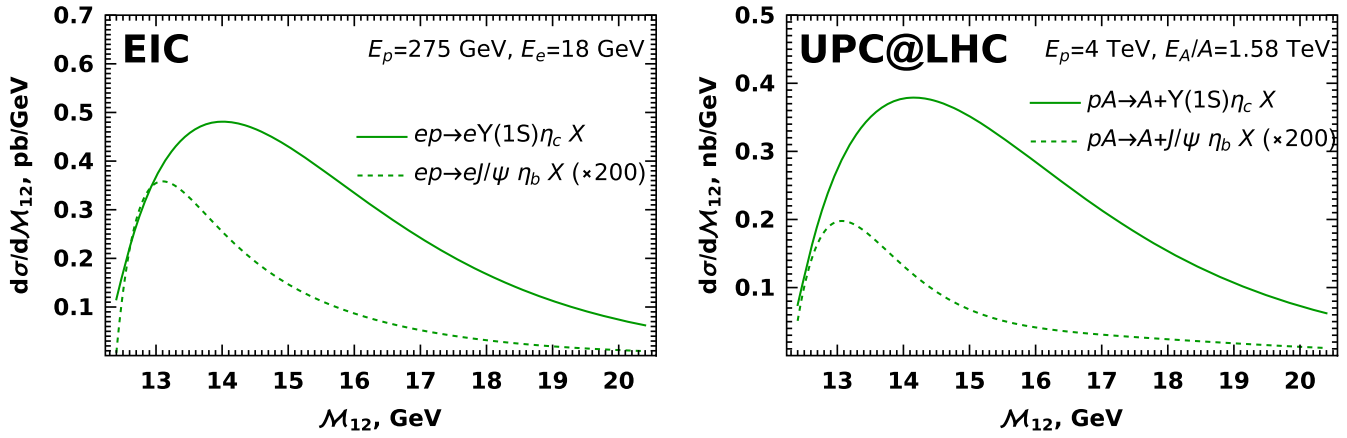

FIG. 9. Single-differential cross-section $d\sigma/d\mathcal{M}_{12}$ as a function of invariant mass $\mathcal{M}_{12}$ of the produced heavy quarkonia pair. For pA collisions the cross section is given on a per nucleon basis, for proton-lead ($^{208}_{82}$Pb) collisions. In order to have comparable magnitudes in different channels, the cross section of $ep \to eJ/\psi\eta_b X$ is multiplied by a common factor 200 in both plots.

luminosity of pA runs at the LHC and will compensate smallness of the cross section.

Since quarkonia are detected via decays into light hadrons, for feasibility analysis it is important to know the total number of experimentally detected events N_d and the counting rates dN_d/dt in a given decay mode. Technically, N_d is merely a product of the total number of produced events $N_{\rm tot}$ by the corresponding quarkonia decay branching fractions,

$$N_d = \mathrm{Br}_1 \times \mathrm{Br}_2 \times N_{\rm tot}. \tag{60}$$

In the last two columns of Table I we provide the values of dN_d/dt and N_d for $\Upsilon\eta_c$ photoproduction, assuming that the

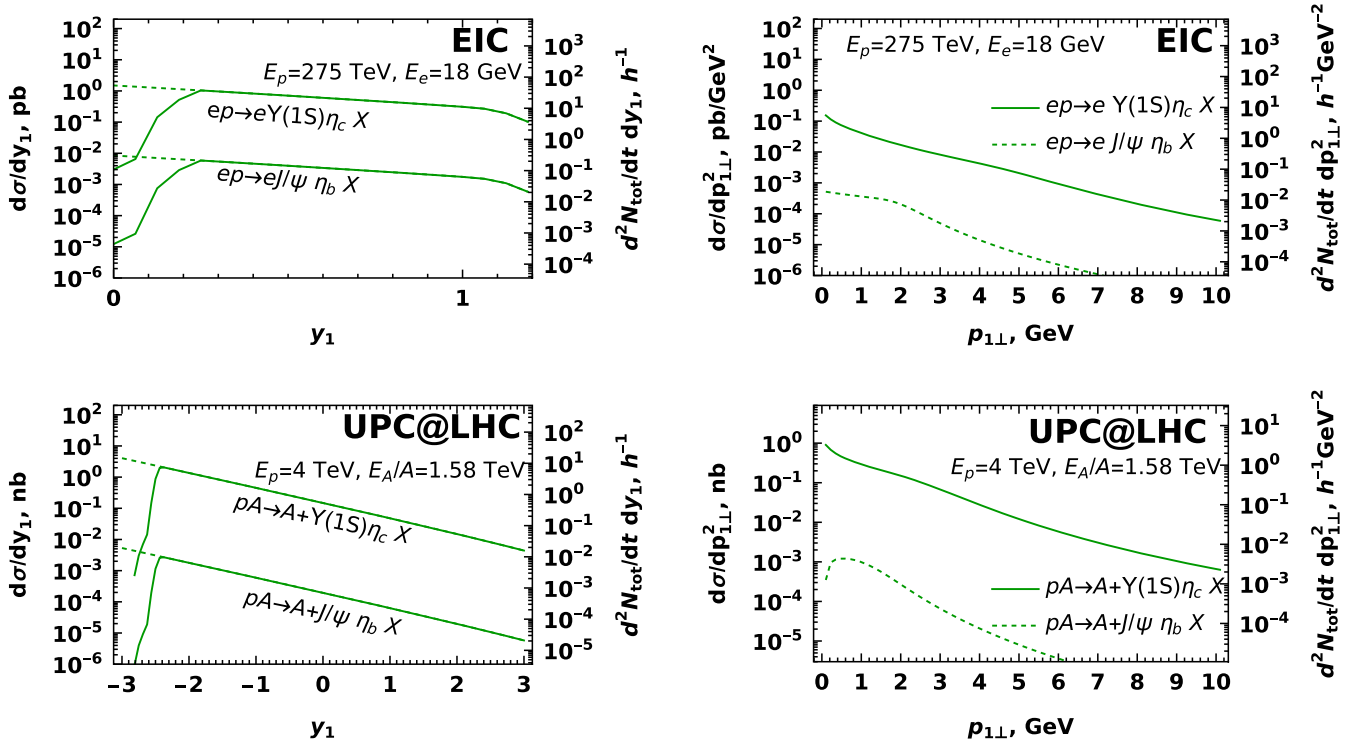

FIG. 10. Single-differential cross sections at the EIC (upper row) and in ultraperipheral kinematics at the LHC (lower row). Left column: rapidity dependence of the cross-section $d\sigma/dy_1$. Solid line corresponds to the cross section with constraint (58); without it the cross sections would follow the dashed line. Right plot: transverse momentum dependence of the cross-section $d\sigma/dp_1^2$. In all plots the scale on the right-hand side shows the quarkonia pair production rates per unit of time (hour) per unit of rapidity (dy_1) or transverse momentum (dp_1^2), assuming the instantaneous luminosities given in Table I. For the pA collisions, the cross sections are given on a per nucleon basis.

quarkonia are detected via $\Upsilon(1S) \to \mu^+\mu^-$, $\eta_c(1S) \to K^0_S K^+\pi^-$ decays and using the branching fractions [94,95]

$$\begin{aligned} \mathrm{Br}_1 &= \mathrm{Br}(\Upsilon(1S) \to \mu^+\mu^-) = 2.48\%, \\ \mathrm{Br}_2 &= \mathrm{Br}(\eta_c(1S) \to K^0_S K^+\pi^-) = 2.6\%. \end{aligned} \tag{61}$$

We could not make similar estimates for $J/\psi\eta_b$ photoproduction because of a lack of experimental data for η_b branching fractions [94], and their theoretically expected smallness for many prospective detection channels [96].

In Fig. 9 we show the single-differential cross-sections $d\sigma/d\mathcal{M}_{12}$, where $\mathcal{M}_{12}$ is the invariant mass of the quarkonia pairs. Finally, in Fig. 10 we show the single-differential cross-sections $d\sigma/dy_1$ and $d\sigma/dp_1$ which characterize distributions of produced vector mesons ($\Upsilon(1S)$ or J/ψ) over rapidities and transverse momenta, assuming that we have integrated out all other kinematic variables. The scale on the right-hand side of each plot in Fig. 10 shows the estimated production rates in the EIC and LHC kinematics, for instantaneous luminosities from Table I. These numbers are sufficiently large, even taking into account small branchings into final state light hadrons.

IV. CONCLUSIONS

In this manuscript we analyzed in detail the inclusive photoproduction of heavy charmonia-bottomonia pairs. We focused on quarkonia pairs with opposite C parities ($\Upsilon\eta_c, J/\psi\eta_b$), which do not require exchange of quantum numbers in the t channel, and thus have the largest cross sections. We found that the cross section is sensitive to bilinear superposition of dipole and quadrupole contributions, which contribute in the same combination $S_4(\boldsymbol{x}_1,\boldsymbol{x}_2,\boldsymbol{x}_3,\boldsymbol{x}_4) - S_2(\boldsymbol{x}_1,\boldsymbol{x}_2) \otimes S_2(\boldsymbol{x}_3,\boldsymbol{x}_4)$ as in inclusive *single* quarkonia production [81]. Due to the possibility of varying independently the momenta of both quarkonia, the suggested process can allow one to get a better understanding of the quadrupole scattering amplitude $S_4(\boldsymbol{x}_1,\boldsymbol{x}_2,\boldsymbol{x}_3,\boldsymbol{x}_4)$. We analyzed the role of the quadrupole scattering using parametrizations available from the literature [83,84] and found that numerically it gives the dominant contribution: its omission decreases the cross section by a factor 2–10 depending on the kinematics. The quadrupole term gives a pronounced dependence on the angle between transverse momenta of the quarkonia, which is almost negligible in its absence.

Numerically, the cross sections of the suggested processes are small, but within reach of the ultraperipheral collision experiments at the LHC and at the future Electron-Ion Collider. The smallness of the cross section happens due to the heavy masses of charm and bottom quarks, which control the sizes of the produced $\bar{c}c$ and $\bar{b}b$ pairs. The suggested mechanism also contributes to charmonia-charmonia production, where its contribution is up to two orders of magnitude larger than for charmonia-bottomonia pairs. However, as explained in Sec. II B, in that channel there are additional contributions which have a significantly more complicated structure and require a separate study.

Potentially, the suggested processes may also be studied in electron-ion (eA) collisions at the EIC and heavy ion (AA) collisions at the LHC in ultraperipheral kinematics, where additional enhancement by atomic mass number A would allow one to achieve much higher yields of quarkonia pairs. Since the modification of the dipole amplitude due to nuclear effects is understood reasonably well [97,98], such process could allow one to study the currently unknown quadrupole scattering amplitude in the heavy nuclei.[3]

ACKNOWLEDGMENTS

We thank our colleagues at Universidad Técnica Federico Santa María for encouraging discussions. This research was partially supported by Proyecto ANID PIA/APOYO AFB230003 (Chile) and Fondecyt (Chile) Grant No. 1220242. Powered@NLHPC. This research was partially supported by the supercomputing infrastructure of the National Laboratory for High Performance Computing (ECM-02).

APPENDIX A: PHOTON WAVE FUNCTION $\psi^{(\gamma)}_{\bar{Q}Q\bar{Q}Q}$

The evaluation of the photon wave function follows the standard light-cone rules formulated in [19,99]. The result for the $\bar{Q}Q$ component is well known from the literature [100,101] and is given by

$$\begin{aligned} \Psi^{\lambda}_{h\bar{h}}(z,\boldsymbol{r}_{12},m_q,a) = -\frac{2}{(2\pi)}\Big[&(z\delta_{\lambda,h} - (1-z)\delta_{\lambda,-h})\delta_{h,-\bar{h}} i\boldsymbol{\epsilon}_\lambda \\ &\cdot\nabla - \frac{m_q}{\sqrt{2}}\mathrm{sign}(h)\delta_{\lambda,h}\delta_{h,\bar{h}}\Big] K_0(a\boldsymbol{r}_{12}), \end{aligned} \tag{A1}$$

where $\lambda, h, \bar{h}$ are the helicities of the incoming photon and outgoing quark, $\epsilon^\mu(q)$ is the polarization vector of the photon, z is the fraction of the photon momentum carried by the quark, and $\boldsymbol{r}_{12}$ is the transverse distance between the quark and antiquark. The wave function of the $\bar{Q}Q\bar{Q}Q$ component can be expressed in terms of the wave function of the $\bar{Q}Q$ component. In what follows we will focus on the photoproduction kinematics, assuming the transverse polarization of the incoming photons. We will use the reference frame in which the photon momentum has only a plus component,

$$q \approx (q^+, 0, \boldsymbol{0}_\perp), \tag{A2}$$

[3]In case of ultraperipheral pA collisions, this problem does not occur because in the chosen kinematics the nucleus acts only as a source of quasireal photons, whereas the 4-quark ensemble propagates in the gluonic field of the proton.

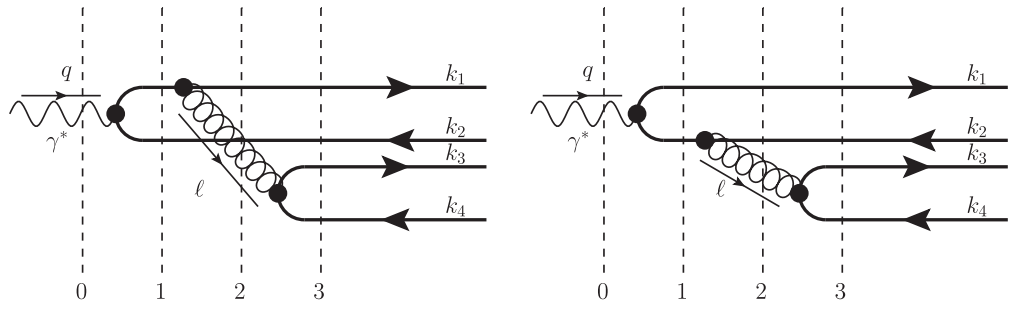

FIG. 11. Leading order contribution to the wave function $\psi^{(\gamma)}_{\bar{Q}Q\bar{Q}Q}$ defined in the text. The momenta k_i shown in the right-hand side are Fourier conjugates of the coordinates x_i. It is implied that both diagrams should be supplemented by all possible permutations of final state quarks (see the text for more details).

so the polarization vector of the incoming photon is given by

$$\varepsilon^{\mu}_{T}(q) \equiv \left(0, \frac{\boldsymbol{q}_{\perp}\cdot\boldsymbol{\epsilon}_{\gamma}}{q^{+}}, \boldsymbol{\epsilon}_{\gamma}\right) \approx (0,0,\boldsymbol{\epsilon}_{\gamma}),$$
$$\boldsymbol{\epsilon}_{\gamma} = \frac{1}{\sqrt{2}}\begin{pmatrix}1\\ \pm i\end{pmatrix}, \qquad \gamma = \pm 1. \tag{A3}$$

In leading order over α_s the wave function obtains contributions from the two diagrams shown in Fig. 11. In what follows we will assume that the produced quark-antiquark pairs have different flavors, and will use the notations m_1 for the current mass of the quark line connected to a photon, and m_2 for the current masses of the quark-antiquark pair produced from the virtual gluon. The evaluation of the diagrams follows the standard rules of the light-cone perturbation theory [19,99]. The detailed evaluation of the $\bar{Q}Q\bar{Q}Q$ component of the photon wave function $\psi^{(\gamma)}_{\bar{Q}Q\bar{Q}Q}$ may be found in [36], and here for the sake of completeness we provide only the final result. This wave function can be represented as a sum

$$\psi^{(\gamma)}_{\bar{Q}Q\bar{Q}Q} = \psi^{(\gamma,\mathrm{noninst})}_{\bar{Q}Q\bar{Q}Q} + \psi^{(\gamma,\mathrm{inst})}_{\bar{Q}Q\bar{Q}Q} \tag{A4}$$

where the first and the second terms correspond to contributions of noninstantaneous and instantaneous parts of propagators of all virtual particles, and for the sake of brevity we omitted color and helicity indices of heavy quarks (c_i and a_i respectively). The noninstantaneous contribution is given by the sum

$$\psi^{(\gamma,\mathrm{noninst})}_{\bar{Q}Q\bar{Q}Q}(\{\alpha_i,\boldsymbol{x}_i\}) = A(\{\alpha_i,\boldsymbol{x}_i\}) + B(\{\alpha_i,\boldsymbol{x}_i\}), \tag{A5}$$

where

$$\begin{aligned}
A(\{\alpha_i,\boldsymbol{r}_i\}) = &-\frac{2e_q\alpha_s(\mu)(t_a)_{c_1c_2}\otimes(t_a)_{c_3c_4}}{\pi^3(1-\alpha_1-\alpha_2)^2\sqrt{\alpha_1\alpha_2}}\int\frac{q_1dq_1k_2dk_2}{\frac{\bar{\alpha}_2q_1^2}{\alpha_1(1-\alpha_1-\alpha_2)}+\frac{m_1^2(\alpha_1+\alpha_2)}{\alpha_1\alpha_2}+\frac{k_2^2}{\alpha_2\bar{\alpha}_2}} \\
&\times\frac{1}{k_2^2+m_1^2}\sqrt{\frac{\bar{\alpha}_2}{\alpha_1}}\Big[(\alpha_2\delta_{\gamma,a_2}-\bar{\alpha}_2\delta_{\gamma,-a_2})(\bar{\alpha}_2\delta_{\lambda,a_1}+\alpha_1\delta_{\lambda,-a_1})\delta_{a_1,-a_2} \\
&\times(\boldsymbol{n}_{2,134}\cdot\boldsymbol{\epsilon}_{\gamma})(\boldsymbol{n}_{1,34}\cdot\boldsymbol{\epsilon}^{*}_{\lambda})k_2J_1(k_2|\boldsymbol{x}_2-\boldsymbol{b}_{134}|)q_1J_1(q_1|\boldsymbol{x}_1-\boldsymbol{b}_{34}|) \\
&+\frac{m_q^2}{2}\delta_{\lambda,-a_1}\delta_{\gamma,a_2}\delta_{a_1,-a_2}J_0(k_2|\boldsymbol{x}_2-\boldsymbol{b}_{134}|)J_0(q_1|\boldsymbol{x}_1-\boldsymbol{b}_{34}|)\frac{(1-\alpha_1-\alpha_2)^2}{1-\alpha_2} \\
&-\frac{im_q}{\sqrt{2}}\mathrm{sign}(a_2)\delta_{\gamma,a_2}\delta_{a_1,a_2}(\bar{\alpha}_2\delta_{\lambda,a_1}+\alpha_1\delta_{\lambda,-a_1})\boldsymbol{n}_{1,34}\cdot\boldsymbol{\epsilon}^{*}_{\lambda}q_1J_1(q_1|\boldsymbol{x}_1-\boldsymbol{b}_{34}|)J_0(k_2|\boldsymbol{x}_2-\boldsymbol{b}_{134}|) \\
&-\frac{im_q}{\sqrt{2}}\mathrm{sign}(a_1)\delta_{\lambda,-a_1}(\alpha_2\delta_{\gamma,a_2}-\bar{\alpha}_2\delta_{\gamma,-a_2})\delta_{a_1,a_2}\frac{(1-\alpha_1-\alpha_2)^2}{1-\alpha_2} \\
&\times(\boldsymbol{n}_{2,134}\cdot\boldsymbol{\epsilon}_{\gamma})k_2J_1(k_2|\boldsymbol{x}_2-\boldsymbol{b}_{134}|)J_0(q_1|\boldsymbol{x}_1-\boldsymbol{b}_{34}|)\Big] \\
&\times\Psi^{-\lambda}_{a_3,a_4}\left(\frac{\alpha_3}{\alpha_3+\alpha_4},\boldsymbol{r}_{34},m_2,\sqrt{m_2^2+\frac{\alpha_3\alpha_4}{\alpha_3+\alpha_4}\left[\frac{\bar{\alpha}_2q_1^2}{\alpha_1(1-\alpha_1-\alpha_2)}+\frac{m_1^2(\alpha_1+\alpha_2)}{\alpha_1\alpha_2}+\frac{k_2^2}{\alpha_2\bar{\alpha}_2}\right]}\right),
\end{aligned} \tag{A6}$$

$$\Psi^{\lambda}_{h\bar{h}}(z,\boldsymbol{r}_{12},m_q,a) = -\frac{2}{(2\pi)}\left[(z\delta_{\lambda,h}-(1-z)\delta_{\lambda,-h})\delta_{h,-\bar{h}}i\boldsymbol{\epsilon}_{\lambda}\cdot\nabla-\frac{m_q}{\sqrt{2}}\mathrm{sign}(h)\delta_{\lambda,h}\delta_{h,\bar{h}}\right]K_0(a\boldsymbol{r}), \tag{A7}$$

and

$$B(\alpha_1,\boldsymbol{x}_1,\alpha_2,\boldsymbol{x}_2,\alpha_3,\boldsymbol{x}_3,\alpha_4,\boldsymbol{x}_4) = -A(\alpha_2,\boldsymbol{x}_2,\alpha_1,\boldsymbol{x}_1,\alpha_4,\boldsymbol{x}_4,\alpha_3,\boldsymbol{x}_3).$$

We also introduced a shorthand notation

$$\boldsymbol{b}_{j_1\ldots j_n} = \frac{\alpha_{j_1}\boldsymbol{x}_{j_1}+\cdots+\alpha_{j_n}\boldsymbol{x}_{j_n}}{\alpha_{j_1}+\cdots+\alpha_{j_n}} \tag{A8}$$

for the center-of-mass position of the n partons $j_1,\ldots j_n$, and

$$\boldsymbol{n}_{i,j_1\ldots j_n} = \frac{\boldsymbol{x}_i-\boldsymbol{b}_{j_1\ldots j_n}}{|\boldsymbol{x}_i-\boldsymbol{b}_{j_1\ldots j_n}|} \tag{A9}$$

for a unit vector pointing from quark i toward the center of mass of the system of quarks $j_1\ldots j_n$. The variables $\boldsymbol{r}_1-\boldsymbol{b}_{34}$ and $\boldsymbol{r}_2-\boldsymbol{b}_{34}$ physically have the meaning of the relative distance between the recoil quark or antiquark and the emitted gluon. Similarly, the variables $\boldsymbol{r}_1-\boldsymbol{b}_{234}$ and $\boldsymbol{r}_2-\boldsymbol{b}_{134}$ might be interpreted as the size of a $\bar{Q}Q$ pair produced right after splitting of the incident photon. For the instantaneous contributions it is possible to get

$$\psi^{(\gamma,\mathrm{inst})}_{\bar{Q}Q\bar{Q}Q}(\{\alpha_i,\boldsymbol{r}_i\}) = A_g(\{\alpha_i,\boldsymbol{r}_i\}) + B_g(\{\alpha_i,\boldsymbol{r}_i\}) + A_q(\{\alpha_i,\boldsymbol{r}_i\}) + B_q(\{\alpha_i,\boldsymbol{r}_i\}), \tag{A10}$$

where the subscript indices q, g in the right-hand side denote the parton propagator which should be taken instantaneous (q for quark, g for gluon), and

$$\begin{aligned} A_g(\{\alpha_i,\boldsymbol{r}_i\}) = &-\frac{e_q\alpha_s(m_Q)(t_a)_{c_1c_2}\otimes(t_a)_{c_3c_4}}{\pi^4(1-\alpha_1-\alpha_2)^3}\int q_1dq_1k_2dk_2J_0(q_1|\boldsymbol{r}_1-\boldsymbol{b}_{34}|)\\ &\times\frac{1}{\boldsymbol{k}_{2\perp}^2+m_1^2}\Big[(\alpha_2\delta_{\gamma,a_1}-\bar{\alpha}_2\delta_{a_1,-\gamma})\delta_{a_1,-a_2}i\boldsymbol{n}_{2,134}\cdot\boldsymbol{\epsilon}_\gamma k_2J_1(k_2|\boldsymbol{r}_2-\boldsymbol{b}_{134}|)\\ &+\frac{m_q}{\sqrt{2}}\mathrm{sign}(a_1)\delta_{\gamma,a_1}\delta_{a_1,a_2}J_0(k_2|\boldsymbol{r}_2-\boldsymbol{b}_{134}|)\Big]\alpha_3\alpha_4\delta_{a_3,-a_4}K_0(a_{34}\boldsymbol{r}_{34}), \end{aligned} \tag{A11}$$

$$\begin{aligned} A_q(\{\alpha_i,\boldsymbol{r}_i\}) = &-\frac{e_q\alpha_s(m_q)(t_a)_{c_1c_2}\otimes(t_a)_{c_3c_4}}{2\pi^4(1-\alpha_1-\alpha_2)^2\bar{\alpha}_2}\delta_{a_1,-a_2}\delta_{\gamma,-a_1}\int q_1dq_1k_2dk_2\frac{J_0(q_1|\boldsymbol{r}_1-\boldsymbol{b}_{34}|)J_0(k_2|\boldsymbol{r}_2-\boldsymbol{b}_{134}|)}{D_2(\alpha_1,\boldsymbol{k}_1;\alpha_2,\boldsymbol{k}_2)}\\ &\times\left[-(\alpha_3\delta_{-\gamma,a_3}-\alpha_4\delta_{\gamma,a_3})\delta_{a_3,-a_4}i\boldsymbol{\epsilon}_\gamma\cdot\boldsymbol{n}_{34}a_{34}K_1(a_{34}\boldsymbol{r}_{34})-\frac{m_q(\alpha_3+\alpha_4)}{\sqrt{2}}\mathrm{sign}(a_3)\delta_{\gamma,-a_3}\delta_{a_3,a_4}K_0(a_{34}\boldsymbol{r}_{34})\right] \end{aligned} \tag{A12}$$

$$a_{34}(q_1,k_2) \equiv \sqrt{m_2^2+\frac{\alpha_3\alpha_4}{\alpha_3+\alpha_4}\left[\frac{\bar{\alpha}_2q_1^2}{\alpha_1(1-\alpha_1-\alpha_2)}+\frac{m_1^2(\alpha_1+\alpha_2)}{\alpha_1\alpha_2}+\frac{k_2^2}{\alpha_2\bar{\alpha}_2}\right]} \tag{A13}$$

and the functions B_q, B_g can be obtained from A_q, A_g using

$$B_i(\alpha_1,\boldsymbol{x}_1,\alpha_2,\boldsymbol{x}_2,\alpha_3,\boldsymbol{x}_3,\alpha_4,\boldsymbol{x}_4) = -A_i(\alpha_2,\boldsymbol{x}_2,\alpha_1,\boldsymbol{x}_1,\alpha_4,\boldsymbol{x}_4,\alpha_3,\boldsymbol{x}_3), \qquad i=q,g. \tag{A14}$$

We can observe that in all terms the dependence on color structure is encoded in a common factor $\sim(t_a)_{c_1c_2}\otimes(t_a)_{c_3c_4}$, which drastically simplifies evaluations and allows one to cast the result in the form of a convolution of wave functions and a dipole amplitude.

APPENDIX B: EVALUATION OF THE MULTIPOLE CORRELATOR

In this section we evaluate the multipole correlator

$$\mathcal{A}^{c_1c_2c_3c_4}_{c_1'c_2'c_3'c_4'}(\boldsymbol{x}_1,\boldsymbol{y}_1,\ldots,\boldsymbol{x}_4,\boldsymbol{y}_4) = \left\langle\prod_{k=1}^{4}[U^\dagger(\boldsymbol{x}_k)U(\boldsymbol{y}_k)]^{c_a}_{c_a'}\right\rangle \tag{B1}$$

where c_a, c_a' are the color indices in fundamental representation of the color group, and angular brackets stand for the color averaging $\int\mathcal{D}\mu[U_x]$. As explained in the text, this amplitude appears when we consider production of two color singlet quarkonia; for color octet channel the matrices $U^\dagger, U$ are separated by additional color generators t^a. Previously, similar correlators have been evaluated exactly in [87,88] in the context of studies of inclusive 3-quark production; for the 4-quark production the result was provided in implicit form (convoluted with hard amplitudes) in the large-N_c limit, when all multipoles are expressed via dipole amplitudes. For the sake of completeness, below we provide a complete result for the amplitude.

Since the target is color singlet, it is expected that color averaging of the right-hand side should eventually include a sum over all possible color singlet irreducible representations which appear in direct product of $U^\dagger U$ matrices, namely

$$\mathcal{A}^{c_1c_2c_3c_4}_{c_1'c_2'c_3'c_4'}(\boldsymbol{x}_1,\boldsymbol{y}_1,\ldots,\boldsymbol{x}_4,\boldsymbol{y}_4) = \sum_{\boldsymbol{p}} \delta^{c_1}_{c_{p_1}'}\delta^{c_2}_{c_{p_2}'}\delta^{c_3}_{c_{p_3}'}\delta^{c_4}_{c_{p_4}'}\, a_{\boldsymbol{p}}(\boldsymbol{x}_1,\boldsymbol{y}_{p_1},\ldots,\boldsymbol{x}_4,\boldsymbol{y}_{p_4}) \quad \text{(B2)}$$

where summation is done over all possible permutations $\boldsymbol{p}$ of numbers (1,2,3,4), and we use a shorthand notation p_k for the kth element of permutation $\boldsymbol{p}$. Overall, expression (B2) includes $4! = 24$ unknown functions $a_{\boldsymbol{p}}(\ldots)$. In order to fix them, we may combine (B1), (B2) and multiply both parts by

$$\delta^{c_1'\ell_1}_{c_1}\delta^{c_2'\ell_2}_{c_2}\delta^{c_3'\ell_3}_{c_3}\delta^{c_4'\ell_4}_{c_4}$$

where $\boldsymbol{\ell} = (\ell_1,\ell_2,\ell_3,\ell_4)$ is some arbitrary fixed permutation. This yields a system of linear inhomogeneous equations

$$\mathcal{M}_{\boldsymbol{\ell},\boldsymbol{p}}\cdot a_{\boldsymbol{p}} = B_{\boldsymbol{\ell}} \quad \text{(B3)}$$

where

$$\mathcal{M}_{\boldsymbol{\ell},\boldsymbol{p}} = \delta^{c_{\ell_1}}_{c_{p_1}}\delta^{c_{\ell_2}}_{c_{p_2}}\delta^{c_{\ell_3}}_{c_{p_3}}\delta^{c_{\ell_4}}_{c_{p_4}}, \quad \text{(B4)}$$

$$B_{\boldsymbol{\ell}} = \left\langle \prod_{k=1}^{4} [U^\dagger(\boldsymbol{x}_k)U(\boldsymbol{y}_k)]^{c_a}_{c_a'} \right\rangle \delta^{c_1'\ell_1}_{c_1}\delta^{c_2'\ell_2}_{c_2}\delta^{c_3'\ell_3}_{c_3}\delta^{c_4'\ell_4}_{c_4}. \quad \text{(B5)}$$

All the elements of the matrix $\mathcal{M}_{\boldsymbol{\ell},\boldsymbol{p}}$ have a very simple structure and are given just by N_c^k, where $1 \le k \le 4$ is the number of disjoint cycles in permutation $\boldsymbol{\ell}\cdot\boldsymbol{p}$. For example, if $\boldsymbol{\ell}_0 = (1,2,3,4)$ and $\boldsymbol{p}_0 = (2,1,4,3)$, then the corresponding element is

$$\mathcal{M}_{\boldsymbol{\ell}_0,\boldsymbol{p}_0} = \delta^{c_1}_{c_2}\delta^{c_2}_{c_1}\delta^{c_3}_{c_4}\delta^{c_4}_{c_3} = N_c^2. \quad \text{(B6)}$$

A contraction of δ symbols in the right-hand side of (B5) allows one to express all elements $B_{\boldsymbol{\ell}}$ in terms of color singlet multitrace operators. For example, for permutations $\boldsymbol{p}_0 = (2,1,4,3)$, $\boldsymbol{p}_1 = (2,3,1,4)$, and $\boldsymbol{p}_2 = (2,3,4,1)$ we may get respectively

$$B_{\boldsymbol{p}_0} = \langle \mathrm{tr}[U^\dagger(\boldsymbol{x}_1)U(\boldsymbol{y}_1)U^\dagger(\boldsymbol{x}_2)U(\boldsymbol{y}_2)]\mathrm{tr}[U^\dagger(\boldsymbol{x}_3)U(\boldsymbol{y}_3)U^\dagger(\boldsymbol{x}_4)U(\boldsymbol{y}_4)]\rangle, \quad \text{(B7)}$$

$$B_{\boldsymbol{p}_1} = \langle \mathrm{tr}[U^\dagger(\boldsymbol{x}_1)U(\boldsymbol{y}_1)U^\dagger(\boldsymbol{x}_2)U(\boldsymbol{y}_2)U^\dagger(\boldsymbol{x}_3)U(\boldsymbol{y}_3)]\mathrm{tr}[U^\dagger(\boldsymbol{x}_4)U(\boldsymbol{y}_4)]\rangle, \quad \text{(B8)}$$

$$B_{\boldsymbol{p}_2} = \langle \mathrm{tr}[U^\dagger(\boldsymbol{x}_1)U(\boldsymbol{y}_1)U^\dagger(\boldsymbol{x}_2)U(\boldsymbol{y}_2)U^\dagger(\boldsymbol{x}_3)U(\boldsymbol{y}_3)U^\dagger(\boldsymbol{x}_4)U(\boldsymbol{y}_4)]\rangle, \quad \text{(B9)}$$

which includes in the right-hand side quadrupole, sextupole, and octupole contributions. The solution of nonlinear system (B3) is straightforward and was done with *Mathematica* (and FeynCalc package [102,103] for color group algebra). The result for the constants $a_{\boldsymbol{p}}$ is very lengthy if written in terms of conventional notations $S_{2n}(x_1)$; for this reason, for the sake of brevity we will introduce shorthand notations,

$$[i] = S_2(\boldsymbol{x}_i,\boldsymbol{y}_i), \qquad [i,j] = S_4(\boldsymbol{x}_i,\boldsymbol{y}_i,\boldsymbol{x}_j,\boldsymbol{y}_j), \qquad [i,j,k] = S_6(\boldsymbol{x}_i,\boldsymbol{y}_i,\boldsymbol{x}_j,\boldsymbol{y}_j,\boldsymbol{x}_k,\boldsymbol{y}_k), \quad \text{(B10)}$$

$$[i,j,k,\ell] = S_8(\boldsymbol{x}_i,\boldsymbol{y}_i,\boldsymbol{x}_j,\boldsymbol{y}_j,\boldsymbol{x}_k,\boldsymbol{y}_k,\boldsymbol{x}_\ell,\boldsymbol{y}_\ell), \quad \text{(B11)}$$

where each of the indices i,j,k,ℓ may take integer values between 1 and 4. In these notations the amplitude $\mathcal{A}$ is written as

$$\begin{aligned}
\mathcal{A}^{c_1c_2c_3c_4}_{c_1'c_2'c_3'c_4'}(\boldsymbol{x}_1,\boldsymbol{y}_1,\ldots,\boldsymbol{x}_4,\boldsymbol{y}_4) &= \frac{\delta^{c_1}_{c_1'}\delta^{c_2}_{c_2'}\delta^{c_3}_{c_3'}\delta^{c_4}_{c_4'}}{N_c^2(N_c^2-7)^2-36}\big[(4-N_c^2)N_c^2(\langle[1][2][3,4]+[1][3][2,4]\rangle \\
&+\langle[1][4][2,3]+[2][4][1,3]+[2][3][1,4]+[3][4][1,2]\rangle)+(N_c^2+6)\langle[1,2][3,4]+[1,4][2,3]+[1,3][2,4]\rangle \\
&+(2N_c^2-3)\langle[1][2,3,4]+[1][2,4,3]+[2][1,3,4]+[2][1,4,3]+[3][1,4,2]+[3][1,2,4]+[4][1,2,3]+[4][1,3,2]\rangle \\
&-5\langle[1,2,3,4]+[1,2,4,3]+[1,3,2,4]+[1,3,4,2]+[1,4,2,3]+[1,4,3,2]\rangle+(N_c^4-8N_c^2+6)N_c^2\langle[1][2][3][4]\rangle] \\
&+\frac{\delta^{c_1}_{c_1'}\delta^{c_2}_{c_2'}\delta^{c_3}_{c_4'}\delta^{c_4}_{c_3'}}{N_c^2(N_c^2-7)^2-36}\Big[(4-N_c^2)N_c^3[1][2][3][4]+N_c(2N_c^2-3)\langle[1][3][2,4]+[1][4][2,3]+[2][3][1,4]+[2][4][1,3]\rangle \\
&+(4-N_c^2)N_c\langle[1][2,3,4]+[1][2,4,3]+[2][1,3,4]+[2][1,4,3]+[1,2][3,4]\rangle+(N_c^4-8N_c^2+6)N_c\langle[1][2][3,4]\rangle
\end{aligned}$$

$$
\begin{aligned}
&+N_c(N_c^2+6)\langle[3][4][1,2]\rangle-5N_c\langle[1,4][2,3]+[1,3][2,4]+[3][1,2,4]+[3][1,4,2]+[4][1,2,3]+[4][1,3,2]\rangle\\
&+\left(2N_c-\frac{3}{N_c}\right)\langle[1,2,3,4]+[1,2,4,3]+[1,3,4,2]+[1,4,3,2]\rangle+\left(N_c+\frac{6}{N_c}\right)\langle[1,3,2,4]+[1,4,2,3]\rangle\Big]\\
&+\frac{\delta^{c_1}_{c_1'}\delta^{c_2}_{c_3'}\delta^{c_3}_{c_2'}\delta^{c_4}_{c_4'}}{N_c(N_c^2(N_c^2-7)^2-36)}[(4-N_c^2)N_c^4\langle[1][2][3][4]\rangle+(N_c^4-8N_c^2+6)N_c^2\langle[1][2,3][4]\rangle\\
&+(N_c^2+6)N_c^2\langle[1,4][2][3]\rangle+(4-N_c^2)N_c^2\langle[1][2,4,3]+[1][2,3,4]+[1,2,3][4]+[1,3,2][4]+[1,4][2,3]\rangle\\
&+(2N_c^2-3)N_c^2\langle[1][2][3,4]+[1,2][3][4]+[2,4][1][3]+[1,3][2][4]\rangle\\
&-5N_c^2\langle[1,2][3,4]+[1,2,4][3]+[1,3,4][2]+[1,4,2][3]+[1,4,3][2]+[1,3][2,4]\rangle\\
&+(2N_c^2-3)\langle[1,2,3,4]+[1,3,2,4]+[1,4,2,3]+[1,4,3,2]\rangle+(N_c^2+6)\langle[1,2,4,3]+[1,3,4,2]\rangle]\\
&+\frac{\delta^{c_1}_{c_1'}\delta^{c_2}_{c_3'}\delta^{c_3}_{c_4'}\delta^{c_4}_{c_2'}}{(N_c^2(N_c^2-7)^2-36)}[(2N_c^2-3)N_c^2\langle[1][2][3][4]\rangle+(4-N_c^2)N_c^2\langle[1][2,4][3]+[1][2][3,4]+[1][2,3][4]\rangle\\
&+\langle[1][2,3,4]\rangle(N_c^4-8N_c^2+6)\\
&+(2N_c^2-3)\langle[1,2][3,4]+[1,3][2,4]+[1,4][2,3]+[1,2,3][4]+[1][2,4,3]+[1,3,4][2]+[1,4,2][3]\rangle\\
&-5N_c^2\langle[1,2][3][4]+[1,3][2][4]+[2][3][1,4]\rangle+(4-N_c^2)\langle[1,2,3,4]+[1,3,4,2]+[1,4,2,3]\rangle\\
&+(N_c^2+6)\langle[1,2,4][3]+[1,3,2][4]+[1,4,3][2]\rangle-5\langle[1,2,4,3]+[1,3,2,4]+[1,4,3,2]\rangle]\\
&+\frac{\delta^{c_1}_{c_1'}\delta^{c_2}_{c_4'}\delta^{c_3}_{c_2'}\delta^{c_4}_{c_3'}}{N_c^2(N_c^2-7)^2-36}[\langle[1][2][3][4]\rangle(2N_c^2-3)N_c^2+\langle[2,4,3][1]\rangle(N_c^4-8N_c^2+6)\\
&+(4-N_c^2)N_c^2\langle[1][2][3,4]+[1][2,3][4]+[1][2,4][3]\rangle+(4-N_c^2)\langle[1,2,4,3]+[1,3,2,4]+[1,4,3,2]\rangle\\
&+(2N_c^2-3)\langle[2,3,4][1]+[1,2,4][3]+[1,3][2,4]+[1,4][2,3]+[1,3,2][4]+[1,2][3,4]+[1,4,3][2]\rangle\\
&+(N_c^2+6)\langle[1,2,3][4]+[1,3,4][2]+[1,4,2][3]\rangle-5N_c^2\langle[1,2][3][4]+[1,3][2][4]+[1,4][2][3]\rangle\\
&-5\langle[1,2,3,4]+[1,3,4,2]+[1,4,2,3]\rangle]\\
&+\frac{\delta^{c_1}_{c_1'}\delta^{c_2}_{c_4'}\delta^{c_3}_{c_3'}\delta^{c_4}_{c_2'}}{N_c(N_c^2(N_c^2-7)^2-36)}[\langle[1][2][3][4]\rangle(4-N_c^2)N_c^4+(2N_c^2-3)N_c^2\langle[1,2][3][4]+[1][2,3][4]+[1][2][3,4]+[1,4][2][3]\rangle\\
&+\langle[2,4][1][3]\rangle(N_c^4-8N_c^2+6)N_c^2+(4-N_c^2)N_c^2\langle[2,3,4][1]+[2,4,3][1]+[1,3][2,4]+[1,2,4][3]+[1,4,2][3]\rangle\\
&-5N_c^2\langle[1,2][3,4]+[1,4][2,3]+[1,2,3][4]+[1,3,4][2]+[1,3,2][4]+[1,4,3][2]\rangle+(N_c^2+6)\langle[1,2,3,4]+[1,4,3,2]\rangle\\
&+(N_c^2+6)N_c^2\langle[1,3][2][4]\rangle+(2N_c^2-3)\langle[1,2,4,3]+[1,3,2,4]+[1,3,4,2]+[1,4,2,3]\rangle]\\
&+\frac{\delta^{c_1}_{c_2'}\delta^{c_2}_{c_1'}\delta^{c_3}_{c_3'}\delta^{c_4}_{c_4'}}{N_c(N_c^2(N_c^2-7)^2-36)}[-(N_c^2-4)N_c^4\langle[1][2][3][4]\rangle+(N_c^2+6)N_c^2\langle[1][2][3,4]\rangle\\
&+(2N_c^2-3)N_c^2\langle[1][2,3][4]+[2,4][1][3]+[1,3][2][4]+[1,4][2][3]\rangle+(N_c^2+6)\langle[1,3,2,4]+[1,4,2,3]\rangle\\
&+N_c^2(4-N_c^2)\langle[1,2][3,4]+[1,2,3][4]+[1,2,4][3]+[1,3,2][4]+[1,4,2][3]\rangle\\
&+\langle[1,2][3][4]\rangle(N_c^4-8N_c^2+6)N_c^2+(2N_c^2-3)\langle[1,2,3,4]+[1,2,4,3]+[1,3,4,2]+[1,4,3,2]\rangle\\
&-5N_c^2\langle[1][2,3,4]+[1][2,4,3]+[2][1,3,4]+[2][1,4,3]+[1,3][2,4]+[1,4][2,3]\rangle]\\
&+\frac{\delta^{c_1}_{c_2'}\delta^{c_2}_{c_1'}\delta^{c_3}_{c_4'}\delta^{c_4}_{c_3'}}{(N_c^2(N_c^2-7)^2-36)}\Big[\langle[1,2][3,4]\rangle(N_c^4-8N_c^2+6)-(N_c^2-4)N_c^2\langle[1][2][3,4]+[1,2][3][4]\rangle\\
&+(N_c^2+6)N_c^2\langle[1][2][3][4]\rangle-5N_c^2\langle[1][2,3][4]+[1][2,4][3]+[1,3][2][4]+[1,4][2][3]\rangle\\
&+(2N_c^2-3)(\langle[2,3,4][1]+[2,4,3][1]+[1,2,3][4]+[1,2,4][3]+[1,3,2][4]+[1,3,4][2]+[1,4,2][3]+[1,4,3][2]\rangle)\\
&+(4-N_c^2)\langle[1,2,3,4]+[1,2,4,3]+[1,3,4,2]+[1,4,3,2]\rangle+(N_c^2+6)\langle[1,3][2,4]+[1,4][2,3]\rangle\\
&-5\langle[1,3,2,4]+[1,4,2,3]\rangle]
\end{aligned}
$$

$$
\begin{aligned}
&+\frac{\delta^{c_1}_{c_2'}\delta^{c_2}_{c_3'}\delta^{c_3}_{c_1'}\delta^{c_4}_{c_4'}}{(N_c^2(N_c^2-7)^2-36)}[(2N_c^2-3)N_c^2\langle[1][2][3][4]\rangle+(4-N_c^2)N_c^2\langle[1][2,3][4]+[1,2][3][4]+[1,3][2][4]\rangle\\
&+(N_c^4-8N_c^2+6)\langle[1,2,3][4]\rangle-5N_c^2\langle[1][2][3,4]+[1][2,4][3]+[1,4][2][3]\rangle\\
&+(2N_c^2-3)(\langle[2,3,4][1]+[1,2,4][3]+[1,3,2][4]+[1,4,3][2]+[1,2][3,4]+[1,3][2,4]+[1,4][2,3]\rangle)\\
&+(N_c^2+6)\langle[2,4,3][1]+[1,3,4][2]+[1,4,2][3]\rangle+(4-N_c^2)\langle[1,2,3,4]+[1,2,4,3]+[1,4,2,3]\rangle\\
&-5(\langle[1,3,2,4]+[1,3,4,2]+[1,4,3,2]\rangle)]\\
&+\frac{\delta^{c_1}_{c_2'}\delta^{c_2}_{c_3'}\delta^{c_3}_{c_4'}\delta^{c_4}_{c_1'}}{N_c(N_c^2(N_c^2-7)^2-36)}[-5N_c^4\langle[1][2][3][4]\rangle+(N_c^4-8N_c^2+6)\langle[1,2,3,4]\rangle+N_c^2(N_c^2+6)\langle[2,4][1][3]+[1,3][2][4]\rangle\\
&+(2N_c^2-3)N_c^2\langle[1][2][3,4]+[1][2,3][4]+[1,2][3][4]+[1,4][2][3]\rangle\\
&+N_c^2(4-N_c^2)\langle[2,3,4][1]+[1,2,4][3]+[1,3,4][2]+[1,2,3][4]+[1,2][3,4]+[1,4][2,3]\rangle\\
&-5N_c^2(\langle[1][2,4,3]\rangle+\langle[1,3][2,4]\rangle+\langle[1,3,2][4]\rangle+\langle[1,4,2][3]\rangle+\langle[1,4,3][2]\rangle)\\
&+(2N_c^2-3)(\langle[1,2,4,3]\rangle+\langle[1,3,2,4]\rangle+\langle[1,3,4,2]\rangle+\langle[1,4,2,3]\rangle)+(N_c^2+6)\langle[1,4,3,2]\rangle]\\
&-5N_c^2\langle[1][2,4,3]+[1,3][2,4]+[1,3,2][4]+[1,4,2][3]+[1,4,3][2]\rangle\\
&+(2N_c^2-3)\langle[1,2,4,3]+[1,3,2,4]+[1,3,4,2]+[1,4,2,3]\rangle+(N_c^2+6)\langle[1,4,3,2]\rangle]\\
&+\frac{\delta^{c_1}_{c_2'}\delta^{c_2}_{c_4'}\delta^{c_3}_{c_1'}\delta^{c_4}_{c_3'}}{N_c(N_c^2(N_c^2-7)^2-36)}[-5N_c^4\langle[1][2][3][4]\rangle+(N_c^2+6)N_c^2\langle[1][2,3][4]+[1,4][2][3]\rangle+(N_c^4-8N_c^2+6)\langle[1,2,4,3]\rangle\\
&+(2N_c^2-3)N_c^2\langle[1][2][3,4]+[2,4][1][3]+[1,2][3][4]+[1,3][2][4]\rangle\\
&-5N_c^2\langle[1][2,3,4]+[1,3,2][4]+[1,3,4][2]+[1,4][2,3]+[1,4,2][3]\rangle\\
&+N_c^2(4-N_c^2)\langle[2,4,3][1]+[1,2][3,4]+[1,3][2,4]+[1,2,3][4]+[1,2,4][3]+[1,4,3][2]\rangle\\
&+(2N_c^2-3)\langle[1,2,3,4]+[1,3,2,4]+[1,4,2,3]+[1,4,3,2]\rangle+(N_c^2+6)\langle[1,3,4,2]\rangle]\\
&+\frac{\delta^{c_1}_{c_2'}\delta^{c_2}_{c_4'}\delta^{c_3}_{c_3'}\delta^{c_4}_{c_1'}}{(N_c^2(N_c^2-7)^2-36)}[\langle[1][2][3][4]\rangle(2N_c^2-3)N_c^2+(4-N_c^2)N_c^2\langle[1][2,4][3]+[1,2][3][4]+[1,4][2][3]\rangle\\
&+(N_c^4-8N_c^2+6)\langle[1,2,4][3]\rangle-5N_c^2\langle[1][2][3,4]+[1][2,3][4]+[1,3][2][4]\rangle\\
&+(N_c^2+6)\langle[2,3,4][1]+[1,3,2][4]+[1,4,3][2]\rangle+(4-N_c^2)\langle[1,2,3,4]+[1,2,4,3]+[1,3,2,4]\rangle\\
&+(2N_c^2-3)\langle[2,4,3][1]+[1,2][3,4]+[1,2,3][4]+[1,3][2,4]+[1,3,4][2]+[1,4][2,3]+[1,4,2][3]\rangle\\
&-5\langle[1,3,4,2]+[1,4,2,3]+[1,4,3,2]\rangle]\\
&+\frac{\delta^{c_1}_{c_3'}\delta^{c_2}_{c_1'}\delta^{c_3}_{c_2'}\delta^{c_4}_{c_4'}}{(N_c^2(N_c^2-7)^2-36)}[(2N_c^2-3)N_c^2\langle[1][2][3][4]\rangle+(4-N_c^2)N_c^2\langle[1][2,3][4]+[1,2][3][4]+[1,3][2][4]\rangle\\
&+(N_c^4-8N_c^2+6)\langle[1,3,2][4]\rangle-5N_c^2\langle[1][2][3,4]+[1][2,4][3]+[1,4][2][3]\rangle\\
&+(2N_c^2-3)\langle[2,4,3][1]+[1,2][3,4]+[1,2,3][4]+[1,4,2][3]+[1,3][2,4]+[1,3,4][2]+[1,4][2,3]\rangle\\
&+\langle[2,3,4][1]+[1,2,4][3]+[1,4,3][2]\rangle(N_c^2+6)+(4-N_c^2)\langle[1,3,2,4]+[1,3,4,2]+[1,4,3,2]\rangle\\
&-5\langle[1,2,3,4]+[1,2,4,3]+[1,4,2,3]\rangle]\\
&+\frac{\delta^{c_1}_{c_3'}\delta^{c_2}_{c_1'}\delta^{c_3}_{c_4'}\delta^{c_4}_{c_2'}}{N_c(N_c^2(N_c^2-7)^2-36)}[-5N_c^4\langle[1][2][3][4]\rangle+(N_c^2+6)N_c^2\langle[1][2,3][4]+[1,4][2][3]\rangle\\
&+\langle[1,3,4,2]\rangle(N_c^4-8N_c^2+6)+(2N_c^2-3)N_c^2\langle[1][2][3,4]+[2,4][1][3]+[1,2][3][4]+[1,3][2][4]\rangle\\
&+N_c^2(4-N_c^2)\langle[2,3,4][1]+[1,2][3,4]+[1,3][2,4]+[1,3,2][4]+[1,3,4][2]+[1,4,2][3]\rangle\\
&-5N_c^2\langle[1][2,4,3]+[1,2,3][4]+[1,2,4][3]+[1,4][2,3]+[1,4,3][2]\rangle\\
&+(2N_c^2-3)\langle[1,2,3,4]+[1,3,2,4]+[1,4,2,3]+[1,4,3,2]\rangle+(N_c^2+6)\langle[1,2,4,3]\rangle]
\end{aligned}
$$

$$
+\frac{\delta^{c_1}_{c_3'}\delta^{c_2}_{c_2'}\delta^{c_3}_{c_1'}\delta^{c_4}_{c_4'}}{N_c(N_c^2(N_c^2-7)^2-36)}\Big[(4-N_c^2)N_c^4\langle[1][2][3][4]\rangle+(N_c^4-8N_c^2+6)N_c^2\langle[1,3][2][4]\rangle
$$
$$
+\langle[2,4][1][3]\rangle(N_c^2+6)N_c^2+(2N_c^2-3)N_c^2\langle[1][2][3,4]+[1][2,3][4]+[1,2][3][4]+[1,4][2][3]\rangle
$$
$$
+N_c^2(4-N_c^2)\langle[1,2,3][4]+[1,3][2,4]+[1,3,2][4]+[1,3,4][2]+[1,4,3][2]\rangle
$$
$$
-5N_c^2\langle[1][2,3,4]+[1][2,4,3]+[1,2,4][3]+[1,4,2][3]+[1,2][3,4]+[1,4][2,3]\rangle
$$
$$
+(N_c^2+6)\langle[1,2,3,4]+[1,4,3,2]\rangle+(2N_c^2-3)\langle[1,2,4,3]+[1,3,2,4]+[1,3,4,2]+[1,4,2,3]\rangle\Big]
$$
$$
+\frac{\delta^{c_1}_{c_3'}\delta^{c_2}_{c_2'}\delta^{c_3}_{c_4'}\delta^{c_4}_{c_1'}}{(N_c^2(N_c^2-7)^2-36)}[\langle[1][2][3][4]\rangle(2N_c^2-3)N_c^2+(N_c^4-8N_c^2+6)\langle[1,3,4][2]\rangle
$$
$$
+(4-N_c^2)N_c^2\langle[1][2][3,4]+[1,3][2][4]+[1,4][2][3]\rangle-5N_c^2\langle[1][2,3][4]+[1][2,4][3]+[1,2][3][4]\rangle
$$
$$
+(2N_c^2-3)\langle[2,3,4][1]+[1,2][3,4]+[1,2,4][3]+[1,3][2,4]+[1,3,2][4]+[1,4][2,3]+[1,4,3][2]\rangle
$$
$$
+(N_c^2+6)\langle[2,4,3][1]+[1,2,3][4]+[1,4,2][3]\rangle+(4-N_c^2)\langle[1,2,3,4]+[1,3,2,4]+[1,3,4,2]\rangle
$$
$$
-5\langle[1,2,4,3]+[1,4,2,3]+[1,4,3,2]\rangle]
$$
$$
+\frac{\delta^{c_1}_{c_3'}\delta^{c_2}_{c_4'}\delta^{c_3}_{c_1'}\delta^{c_4}_{c_2'}}{(N_c^2(N_c^2-7)^2-36)}[\langle[1][2][3][4]\rangle N_c^2(N_c^2+6)+(N_c^4-8N_c^2+6)\langle[1,3][2,4]\rangle+N_c^2(4-N_c^2)\langle[2,4][1][3]+[1,3][2][4]\rangle
$$
$$
+(2N_c^2-3)\langle[2,3,4][1]+[2,4,3][1]+[1,2,3][4]+[1,2,4][3]+[1,3,2][4]+[1,3,4][2]+[1,4,2][3]+[1,4,3][2]\rangle
$$
$$
+(N_c^2+6)\langle[1,2][3,4]+[1,4][2,3]\rangle+(4-N_c^2)\langle[1,2,4,3]+[1,3,2,4]+[1,3,4,2]+[1,4,2,3]\rangle
$$
$$
-5N_c^2\langle[1][2][3,4]+[1][2,3][4]+[1,2][3][4]+[1,4][2][3]\rangle-5\langle[1,2,3,4]+[1,4,3,2]\rangle]
$$
$$
+\frac{\delta^{c_1}_{c_3'}\delta^{c_2}_{c_4'}\delta^{c_3}_{c_2'}\delta^{c_4}_{c_1'}}{N_c(N_c^2(N_c^2-7)^2-36)}[-5N_c^4[1][2][3][4]+(N_c^4-8N_c^2+6)\langle[1,3,2,4]\rangle+(N_c^2+6)N_c^2\langle[1][2][3,4]+[1,2][3][4]\rangle
$$
$$
+(2N_c^2-3)N_c^2\langle[1][2,3][4]+[2,4][1][3]+[1,3][2][4]+[1,4][2][3]\rangle
$$
$$
-5N_c^2\langle[1][2,3,4]+[1,2][3,4]+[1,2,3][4]+[1,4,2][3]+[1,4,3][2]\rangle
$$
$$
+N_c^2(4-N_c^2)\langle[2,4,3][1]+[1,2,4][3]+[1,3][2,4]+[1,3,2][4]+[1,3,4][2]+[1,4][2,3]\rangle
$$
$$
+(2N_c^2-3)\langle[1,2,3,4]+[1,2,4,3]+[1,3,4,2]+[1,4,3,2]\rangle+(N_c^2+6)\langle[1,4,2,3]\rangle]
$$
$$
+\frac{\delta^{c_1}_{c_4'}\delta^{c_2}_{c_1'}\delta^{c_3}_{c_2'}\delta^{c_4}_{c_3'}}{N_c(N_c^2(N_c^2-7)^2-36)}[-5N_c^4\langle[1][2][3][4]\rangle+(2N_c^2-3)N_c^2\langle[1][2][3,4]+[1][2,3][4]+[1,2][3][4]+[1,4][2][3]\rangle
$$
$$
+(N_c^4-8N_c^2+6)\langle[1,4,3,2]\rangle-5N_c^2\langle[1][2,3,4]+[1,2,3][4]+[1,2,4][3]+[1,3][2,4]+[1,3,4][2]\rangle
$$
$$
+N_c^2(4-N_c^2)\langle[2,4,3][1]+[1,2][3,4]+[1,3,2][4]+[1,4][2,3]+[1,4,2][3]+[1,4,3][2]\rangle
$$
$$
+N_c^2(N_c^2+6)\langle[2,4][1][3]+[1,3][2][4]\rangle+(2N_c^2-3)\langle[1,2,4,3]+[1,3,2,4]+[1,3,4,2]+[1,4,2,3]\rangle
$$
$$
+(N_c^2+6)\langle[1,2,3,4]\rangle]
$$
$$
+\frac{\delta^{c_1}_{c_4'}\delta^{c_2}_{c_1'}\delta^{c_3}_{c_3'}\delta^{c_4}_{c_2'}}{(N_c^2(N_c^2-7)^2-36)}[(2N_c^2-3)N_c^2\langle[1][2][3][4]\rangle+(N_c^4-8N_c^2+6)\langle[1,4,2][3]\rangle
$$
$$
-5N_c^2\langle[1][2][3,4]+[1][2,3][4]+[1,3][2][4]\rangle
$$
$$
+(2N_c^2-3)\langle[2,3,4][1]+[1,2][3,4]+[1,2,4][3]+[1,3][2,4]+[1,3,2][4]+[1,4][2,3]+[1,4,3][2]\rangle
$$
$$
+N_c^2(4-N_c^2)\langle[1][2,4][3]+[1,2][3][4]+[1,4][2][3]\rangle+(4-N_c^2)\langle[1,3,4,2]+[1,4,2,3]+[1,4,3,2]\rangle
$$
$$
+(N_c^2+6)\langle[2,4,3][1]+[1,2,3][4]+[1,3,4][2]\rangle-5\langle[1,2,3,4]+[1,2,4,3]+[1,3,2,4]\rangle]
$$
$$
+\frac{\delta^{c_1}_{c_4'}\delta^{c_2}_{c_2'}\delta^{c_3}_{c_1'}\delta^{c_4}_{c_3'}}{(N_c^2(N_c^2-7)^2-36)}[\langle[1][2][3][4]\rangle(2N_c^2-3)N_c^2+(4-N_c^2)N_c^2\langle[1][2][3,4]+[1,3][2][4]+[1,4][2][3]\rangle
$$
$$
+\langle[1,4,3][2]\rangle(N_c^4-8N_c^2+6)+(N_c^2+6)\langle[2,3,4][1]+[1,2,4][3]+[1,3,2][4]\rangle
$$

$$
\begin{aligned}
&- 5N_c^2\langle[1][2,3][4]+[1][2,4][3]+[1,2][3][4]\rangle+(4-N_c^2)\langle[1,2,4,3]+[1,3,4,2]+[1,4,2,3]+[1,4,3,2]\rangle\\
&+(2N_c^2-3)\langle[2,4,3][1]+[1,2][3,4]+[1,2,3][4]+[1,3][2,4]+[1,3,4][2]+[1,4][2,3]+[1,4,2][3]\rangle\\
&-5\langle[1,2,3,4]+[1,3,2,4]\rangle]\\
&+\frac{\delta^{c_1}_{c_4'}\delta^{c_2}_{c_2'}\delta^{c_3}_{c_3'}\delta^{c_4}_{c_1'}}{N_c(N_c^2(N_c^2-7)^2-36)}[(4-N_c^2)N_c^4\langle[1][2][3][4]\rangle+(N_c^4-8N_c^2+6)N_c^2\langle[1,4][2][3]\rangle\\
&+(2N_c^2-3)N_c^2\langle[1][2][3,4]+[2,4][1][3]+[1,2][3][4]+[1,3][2][4]\rangle+\langle[1][2,3][4]\rangle(N_c^2+6)N_c^2\\
&+(4-N_c^2)N_c^2\langle[1,2,4][3]+[1,3,4][2]+[1,4][2,3]+[1,4,2][3]+[1,4,3][2]\rangle\\
&-5N_c^2\langle[1][2,3,4]+[1][2,4,3]+[1,2][3,4]+[1,2,3][4]+[1,3][2,4]+[1,3,2][4]\rangle\\
&+(2N_c^2-3)\langle[1,2,3,4]+[1,3,2,4]+[1,4,2,3]+[1,4,3,2]\rangle+(N_c^2+6)\langle[1,2,4,3]+[1,3,4,2]\rangle]\\
&+\frac{\delta^{c_1}_{c_4'}\delta^{c_2}_{c_3'}\delta^{c_3}_{c_1'}\delta^{c_4}_{c_2'}}{N_c(N_c^2(N_c^2-7)^2-36)}[-5N_c^4\langle[1][2][3][4]\rangle+(N_c^4-8N_c^2+6)\langle[1,4,2,3]\rangle\\
&+(N_c^2+6)N_c^2\langle[1][2][3,4]+[1,2][3][4]\rangle+(2N_c^2-3)N_c^2\langle[1][2,3][4]+[2,4][1][3]+[1,3][2][4]+[1,4][2][3]\rangle\\
&+N_c^2(4-N_c^2)(\langle[2,3,4][1]+[1,2,3][4]+[1,3][2,4]+[1,4][2,3]+[1,4,2][3]+[1,4,3][2]\rangle)\\
&-5N_c^2\langle[1][2,4,3]+[1,2][3,4]+[1,2,4][3]+[1,3,2][4]+[1,3,4][2]\rangle\\
&+(2N_c^2-3)\langle[1,2,3,4]+[1,2,4,3]+[1,3,4,2]+[1,4,3,2]\rangle+(N_c^2+6)\langle[1,3,2,4]\rangle]\\
&+\frac{\delta^{c_1}_{c_4'}\delta^{c_2}_{c_3'}\delta^{c_3}_{c_2'}\delta^{c_4}_{c_1'}}{(N_c^2(N_c^2-7)^2-36)}[\langle[1][2][3][4]\rangle(N_c^2+6)N_c^2+\langle[1,4][2,3]\rangle(N_c^4-8N_c^2+6)\\
&+(4-N_c^2)N_c^2\langle[1][2,3][4]+[1,4][2][3]\rangle-5N_c^2\langle[1][2][3,4]+[1][2,4][3]+[1,2][3][4]+[1,3][2][4]\rangle\\
&+(2N_c^2-3)\langle[2,3,4][1]+[2,4,3][1]+[1,2,3][4]+[1,2,4][3]+[1,3,2][4]+[1,3,4][2]+[1,4,2][3]+[1,4,3][2]\rangle\\
&+(N_c^2+6)\langle[1,2][3,4]+[1,3][2,4]\rangle+(4-N_c^2)\langle[1,2,3,4]+[1,3,2,4]+[1,4,2,3]+[1,4,3,2]\rangle\\
&-5(\langle[1,2,4,3]+[1,3,4,2]\rangle)].
\end{aligned}
\tag{B12}
$$

We need to mention that each term in the sum (B12) after contraction with partonic amplitudes can contribute with a different factor N_c^n, $n\in\mathbb{N}$; for this reason it might be incorrect to take the limit $N_c\to\infty$ directly in (B12). As can be seen from Fig. 2 and (37), for diagrams 5 and 6 we will need only the amplitude convoluted with color group generators

$$
\mathcal{A}=(t_{a_1})^{c_1'}_{c_1}(t_{a_1})^{c_2'}_{c_2}(t_{a_1})^{c_3'}_{c_3}(t_{a_1})^{c_4'}_{c_4}\mathcal{A}^{c_1c_2c_3c_4}_{c_1'c_2'c_3'c_4'}. \tag{B13}
$$

Using Fierz identity

$$
(t_{a_1})^{c_1'}_{c_1}(t_{a_1})^{c_2'}_{c_2}=\delta^{c_1'}_{c_2}\delta^{c_2'}_{c_1}-\frac{1}{N_c}\delta^{c_1'}_{c_1}\delta^{c_2'}_{c_2} \tag{B14}
$$

and performing convolutions with the help of FeynCalc, we may obtain a surprisingly simple result,

$$
\begin{aligned}
\mathcal{A}&=\langle([1,2]-[1][2])([3,4]-[3][4])\rangle\\
&=\langle(S_4(\boldsymbol{x}_1,\boldsymbol{y}_1,\boldsymbol{x}_2,\boldsymbol{y}_2)-S_2(\boldsymbol{x}_1,\boldsymbol{y}_1)S_2(\boldsymbol{x}_2,\boldsymbol{y}_2))\\
&\quad\times(S_4(\boldsymbol{x}_3,\boldsymbol{y}_3,\boldsymbol{x}_4,\boldsymbol{y}_4)-S_2(\boldsymbol{x}_3,\boldsymbol{y}_3)S_2(\boldsymbol{x}_4,\boldsymbol{y}_4))\rangle,
\end{aligned}
\tag{B15}
$$

namely all the contributions of sextupoles and octupoles cancel in the final result. This is an untrivial property of the photoproduction by a color singlet photon: such cancellation does not occur if we consider *hadroproduction* or production of color octet $\bar{Q}Q$ pairs. Note that the results of this appendix are exact, namely we have not used the large-N_c limit so far.

[1] J. G. Korner and G. Thompson, The heavy mass limit in field theory and the heavy quark effective theory, Phys. Lett. B **264**, 185 (1991).

[2] M. Neubert, Heavy quark symmetry, Phys. Rep. **245**, 259 (1994).

[3] G. T. Bodwin, E. Braaten, and G. P. Lepage, Rigorous QCD analysis of inclusive annihilation and production of heavy quarkonium, Phys. Rev. D **51**, 1125 (1995); **55**, 5853(E) (1997).

[4] F. Maltoni, M. L. Mangano, and A. Petrelli, Quarkonium photoproduction at next-to-leading order, Nucl. Phys. **B519**, 361 (1998).

[5] P. L. Cho and A. K. Leibovich, Color-octet quarkonia production. II, Phys. Rev. D **53**, 6203 (1996).

[6] P. L. Cho and A. K. Leibovich, Color-octet quarkonia production, Phys. Rev. D **53**, 150 (1996).

[7] S. P. Baranov, Highlights from the k_T-factorization approach on the quarkonium production puzzles, Phys. Rev. D **66**, 114003 (2002).

[8] S. P. Baranov and A. Szczurek, Inclusive production of J/ψ meson in proton-proton collisions at BNL RHIC, Phys. Rev. D **77**, 054016 (2008).

[9] S. P. Baranov and A. V. Lipatov, Prompt charmonia production and polarization at the LHC in the NRQCD with k_T-factorization. III. J/ψ meson, Phys. Rev. D **96**, 034019 (2017).

[10] S. P. Baranov, A. V. Lipatov, and N. P. Zotov, Prompt charmonia production and polarization at LHC in the NRQCD with k_T-factorization. Part I: $\psi(2S)$ meson, Eur. Phys. J. C **75**, 455 (2015).

[11] S. P. Baranov, A. V. Lipatov, and N. P. Zotov, Prompt J/ψ production at the LHC: New evidence for the k_T factorization, Phys. Rev. D **85**, 014034 (2012).

[12] Y. Feng, J. P. Lansberg, and J. X. Wang, Energy dependence of direct-quarkonium production in pp collisions from fixed-target to LHC energies: complete one-loop analysis, Eur. Phys. J. C **75**, 313 (2015).

[13] N. Brambilla *et al.*, Heavy quarkonium: Progress, puzzles, and opportunities, Eur. Phys. J. C **71**, 1534 (2011).

[14] H. Han, Y. Q. Ma, C. Meng, H. S. Shao, and K. T. Chao, η_c production at LHC and indications on the understanding of J/ψ production, Phys. Rev. Lett. **114**, 092005 (2015).

[15] H. S. Shao, H. Han, Y. Q. Ma, C. Meng, Y. J. Zhang, and K. T. Chao, Yields and polarizations of prompt J/ψ and $\psi(2S)$ production in hadronic collisions, J. High Energy Phys. 05 (2015) 103.

[16] M. Butenschoen, Z. G. He, and B. A. Kniehl, η_c production at the LHC challenges nonrelativistic-QCD factorization, Phys. Rev. Lett. **114**, 092004 (2015).

[17] E. Braaten, B. A. Kniehl, and J. Lee, Polarization of prompt J/ψ at the Fermilab Tevatron, Phys. Rev. D **62**, 094005 (2000).

[18] S. J. Brodsky, G. Kopp, and P. M. Zerwas, Hadron production near threshold in photon-photon collisions, Phys. Rev. Lett. **58**, 443 (1987).

[19] G. P. Lepage and S. J. Brodsky, Exclusive processes in perturbative quantum chromodynamics, Phys. Rev. D **22**, 2157 (1980).

[20] C. Berger and W. Wagner, Photon-photon reactions, Phys. Rep. **146**, 1 (1987).

[21] M. S. Baek, S. Y. Choi, and H. S. Song, Exclusive heavy meson pair production at large recoil, Phys. Rev. D **50**, 4363 (1994).

[22] P. Ko, C. Yu, and J. Lee, Inclusive double-quarkonium production at the Large Hadron Collider, J. High Energy Phys. 01 (2011) 070.

[23] A. K. Likhoded, A. V. Luchinsky, and S. V. Poslavsky, Simultaneous production of charmonium and bottomonium mesons at the LHC, Phys. Rev. D **91**, 114016 (2015).

[24] H. S. Shao and Y. J. Zhang, Complete study of hadroproduction of a Υ meson associated with a prompt J/ψ, Phys. Rev. Lett. **117**, 062001 (2016).

[25] R. Aaij *et al.* (LHCb Collaboration), Associated production of prompt J/ψ and Υ mesons in pp collisions at $\sqrt{s} = 13$ TeV, J. High Energy Phys. 08 (2023) 093.

[26] V. M. Abazov *et al.* (D0 Collaoration), Evidence for simultaneous production of J/ψ and Υ mesons, Phys. Rev. Lett. **116**, 082002 (2016).

[27] I. Belyaev and D. Savrina, Study of double parton scattering processes with heavy quarks, Adv. Ser. Dir. High Energy Phys. **29**, 141 (2018).

[28] J. P. Lansberg and H. S. Shao, Associated production of a quarkonium and a Z boson at one loop in a quark-hadron-duality approach, J. High Energy Phys. 10 (2016) 153.

[29] J. P. Lansberg, New observables in inclusive production of quarkonia, Phys. Rep. **889**, 1 (2020).

[30] V. P. Goncalves, B. D. Moreira, and F. S. Navarra, Double vector meson production in $\gamma\gamma$ interactions at hadronic colliders, Eur. Phys. J. C **76**, 103 (2016).

[31] V. P. Goncalves and R. Palota da Silva, Exclusive and diffractive quarkonium-pair production at the LHC and FCC, Phys. Rev. D **101**, 034025 (2020).

[32] V. P. Goncalves and M. V. T. Machado, Dipole model for double meson production in two-photon interactions at high energies, Eur. Phys. J. C **49**, 675 (2007).

[33] S. Baranov, A. Cisek, M. Klusek-Gawenda, W. Schafer, and A. Szczurek, The $\gamma\gamma \to J/\psi J/\psi$ reaction and the $J/\psi J/\psi$ pair production in exclusive ultraperipheral ultrarelativistic heavy ion collisions, Eur. Phys. J. C **73**, 2335 (2013).

[34] H. Yang, Z. Q. Chen, and C. F. Qiao, NLO QCD corrections to exclusive quarkonium-pair production in photon-photon collision, Eur. Phys. J. C **80**, 806 (2020).

[35] V. P. Goncalves, B. D. Moreira, and F. S. Navarra, Double vector meson production in photon-hadron interactions at hadronic colliders, Eur. Phys. J. C **76**, 388 (2016).

[36] S. Andrade, M. Siddikov, and I. Schmidt, Exclusive photoproduction of heavy quarkonia pairs, Phys. Rev. D **105**, 076022 (2022).

[37] S. Andrade, M. Siddikov, and I. Schmidt, Exclusive photoproduction of $B_c^{\pm}$ and bottomonia pairs, Eur. Phys. J. C **83**, 457 (2023).

[38] M. Siddikov and I. Schmidt, Exclusive production of quarkonia pairs in collinear factorization framework, Phys. Rev. D **107**, 034037 (2023).

[39] M. Siddikov and I. Schmidt, Exclusive photoproduction of D-meson pairs with large invariant mass, Phys. Rev. D **108**, 096031 (2023).

[40] A. Accardi *et al.*, Electron-Ion Collider: The next QCD frontier, Eur. Phys. J. A **52**, 268 (2016).
[41] R. Abdul Khalek *et al.*, Science requirements and detector concepts for the electron-ion collider: EIC yellow report, Nucl. Phys. **A1026**, 122447 (2022).
[42] J. L. Abelleira Fernandez *et al.* (LHeC Study Group), A large hadron electron collider at CERN, J. Phys. G **39**, 075001 (2012).
[43] M. Mangano, CERN yellow reports: Monographs, arXiv:1710.06353.
[44] P. Agostini *et al.* (LHeC and FCC-he Study Group), The large hadron-electron collider at the HL-LHC, J. Phys. G **48**, 110501 (2021).
[45] A. Abada *et al.* (FCC Collaoration), FCC physics opportunities, Eur. Phys. J. C **79**, 474 (2019).
[46] L. V. Gribov, E. M. Levin, and M. G. Ryskin, Semihard processes in QCD, Phys. Rep. **100**, 1 (1983).
[47] L. D. McLerran and R. Venugopalan, Computing quark and gluon distribution functions for very large nuclei, Phys. Rev. D **49**, 2233 (1994).
[48] L. D. McLerran and R. Venugopalan, Gluon distribution-functions for very large nuclei at small transverse momentum, Phys. Rev. D **49**, 3352 (1994).
[49] L. D. McLerran and R. Venugopalan, Green's functionin the color field of a large nucleus, Phys. Rev. D **50**, 2225 (1994).
[50] A. H. Mueller and J. Qiu, Gluon recombination and shadowing at small values of x, Nucl. Phys. **B268**, 427 (1986).
[51] L. McLerran and R. VenugopalanFock space distributions, structure functions, higher twists, and small x, Phys. Rev. D **59**, 09400 (1999).
[52] K. J. Golec-Biernat and M. Wusthoff, Saturation in diffractive deep inelastic scattering, Phys. Rev. D **60**, 114023 (1999).
[53] B. Z. Kopeliovich and A. V. Tarasov, Gluon shadowing in heavy flavor production off nuclei, Nucl. Phys. **A710**, 180 (2002).
[54] B. Kopeliovich, A. Tarasov, and J. Hufner, Coherence phenomena in charmonium production off nuclei at the energies of RHIC and LHC, Nucl. Phys. **A696**, 669 (2001).
[55] F. Gelis, E. Iancu, J. Jalilian-Marian, and R. Venugopalan, The color glass condensate, Annu. Rev. Nucl. Part. Sci. **60**, 463 (2010).
[56] E. Iancu and A. H. Mueller, From color glass to color dipoles in high-energy onium onium scattering, Nucl. Phys. **A730**, 460 (2004).
[57] Y. V. Kovchegov, Small x F(2) structure function of a nucleus including multiple pomeron exchanges, Phys. Rev. D **60**, 034008 (1999).
[58] Y. V. Kovchegov and H. Weigert, Triumvirate of running couplings in small-x evolution, Nucl. Phys. **A784**, 188 (2007).
[59] I. Balitsky and G. A. Chirilli, Next-to-leading order evolution of color dipoles, Phys. Rev. D **77**, 014019 (2008).
[60] Y. V. Kovchegov and E. Levin, Quantum chromodynamics at high energy, Cambridge Monogr. Part. Phys., Nucl. Phys., Cosmol. **33**, 1 (2012).
[61] I. Balitsky, Effective field theory for the small x evolution, Phys. Lett. B **518**, 235 (2001).
[62] F. Cougoulic and Y. V. Kovchegov, Helicity-dependent generalization of the JIMWLK evolution, Phys. Rev. D **100**, 114020 (2019).
[63] C. A. Aidala *et al.*, Probing nucleons and nuclei in high energy collisions, arXiv:2002.12333.
[64] Y. Q. Ma and R. Venugopalan, Comprehensive description of J/ψ production in proton-proton collisions at collider energies, Phys. Rev. Lett. **113**, 192301 (2014).
[65] V. M. Budnev, I. F. Ginzburg, G. V. Meledin, and V. G. Serbo, The two photon particle production mechanism. Physical problems. Applications. Equivalent photon approximation, Phys. Rep. **15**, 181 (1975).
[66] A. Ayala, M. Hentschinski, J. Jalilian-Marian, and M. E. Tejeda-Yeomans, Spinor helicity methods in high-energy factorization: Efficient momentum-space calculations in the color glass condensate formalism, Nucl. Phys. **B920**, 232 (2017).
[67] P. Caucal, F. Salazar, and R. Venugopalan, Dijet impact factor in DIS at next-to-leading order in the color glass condensate, J. High Energy Phys. 11 (2021) 222.
[68] P. Caucal, F. Salazar, B. Schenke, and R. Venugopalan, Back-to-back inclusive dijets in DIS at small x: Sudakov suppression and gluon saturation at NLO, J. High Energy Phys. 11 (2022) 169.
[69] S. P. Baranov, A. V. Lipatov, and A. A. Prokhorov, Charm fragmentation and associated $J/\psi + Z/W^{\pm}$ production at the LHC, Phys. Rev. D **104**, 034018 (2021).
[70] E. Braaten and T. C. Yuan, Gluon fragmentation into heavy quarkonium, Phys. Rev. Lett. **71**, 1673 (1993).
[71] Z. B. Kang, E. Li, and F. Salazar, Direct quarkonium-plus-gluon production in DIS in the color glass condensate, J. High Energy Phys. 03 (2024) 027.
[72] A. Ayala, M. Hentschinski, J. Jalilian-Marian, and M. E. Tejeda-Yeomans, Polarized 3 parton production in inclusive DIS at small x, Phys. Lett. B **761**, 229 (2016).
[73] S. P. Baranov and A. V. Lipatov, Are there any challenges in the charmonia production and polarization at the LHC?, Phys. Rev. D **100**, 114021 (2019).
[74] Y. Feng, B. Gong, L. P. Wan, and J. X. Wang, An updated study of Υ production and polarization at the Tevatron and LHC, Chin. Phys. C **39**, 123102 (2015).
[75] N. A. Abdulov and A. V. Lipatov, Bottomonium production and polarization in the NRQCD with k_T-factorization. III: $\Upsilon(1S)$ and $\chi_b(1P)$ mesons, Eur. Phys. J. C **81**, 1085 (2021).
[76] A. V. Belitsky, X. Ji, and F. Yuan, Final state interactions and gauge invariant parton distributions, Nucl. Phys. **B656**, 165 (2003).
[77] H. Kowalski and D. Teaney, Impact parameter dipole saturation model, Phys. Rev. D **68**, 114005 (2003).
[78] H. Kowalski, L. Motyka, and G. Watt, Exclusive diffractive processes at HERA within the dipole picture, Phys. Rev. D **74**, 074016 (2006).
[79] J. Bartels, K. J. Golec-Biernat, and K. Peters, On the dipole picture in the nonforward direction, Acta Phys. Pol. B **34**, 3051 (2003), https://www.actaphys.uj.edu.pl/R/34/6/3051/pdf.
[80] D. Yu. Ivanov, A. Schafer, L. Szymanowski, and G. Krasnikov, Exclusive photoproduction of a heavy vector meson in QCD, Eur. Phys. J. C **34**, 297 (2004).

[81] Z. B. Kang, Y. Q. Ma, and R. Venugopalan, Quarkonium production in high energy proton-nucleus collisions: CGC meets NRQCD, J. High Energy Phys. 01 (2014) 056.
[82] A. H. Rezaeian and I. Schmidt, Impact-parameter dependent color glass condensate dipole model and new combined HERA data, Phys. Rev. D **88**, 074016 (2013).
[83] E. Iancu and D. N. Triantafyllopoulos, JIMWLK evolution in the Gaussian approximation, J. High Energy Phys. 04 (2012) 025.
[84] E. Iancu and D. N. Triantafyllopoulos, Higher-point correlations from the JIMWLK evolution, J. High Energy Phys. 11 (2011) 105.
[85] E. Iancu, QCD in heavy ion collisions, arXiv:1205.0579.
[86] P. Agostini, T. Altinoluk, and N. Armesto, Multi-particle production in proton-nucleus collisions in the color glass condensate, Eur. Phys. J. C **81**, 760 (2021).
[87] A. Kovner and A. H. Rezaeian, Double parton scattering in the CGC: Double quark production and effects of quantum statistics, Phys. Rev. D **96**, 074018 (2017).
[88] A. Kovner and A. H. Rezaeian, Multiquark production in $p + A$ collisions: Quantum interference effects, Phys. Rev. D **97**, 074008 (2018).
[89] A. H. Rezaeian, M. Siddikov, M. Van de Klundert, and R. Venugopalan, Analysis of combined HERA data in the impact-parameter dependent saturation model, Phys. Rev. D **87**, 034002 (2013).
[90] E. Eichten, K. Gottfried, T. Kinoshita, K. D. Lane, and T. M. Yan, Charmonium: The model, Phys. Rev. D **17**, 3090 (1978); **21**, 313(E) (1980).
[91] E. Eichten, K. Gottfried, T. Kinoshita, K. D. Lane, and T. M. Yan, Charmonium: Comparison with experiment, Phys. Rev. D **21**, 203 (1980).
[92] C. Quigg and J. L. Rosner, Quarkonium level spacings, Phys. Lett. **71B**, 153 (1977).
[93] A. Martin, A fit of upsilon and charmonium spectra, Phys. Lett. **93B**, 338 (1980).
[94] R. L. Workman *et al.* (Particle Data Group Collaoration), Review of particle physics, Prog. Theor. Exp. Phys. **2022**, 083C01 (2022).
[95] M. Ablikim *et al.* (BESIII Collaoration), Measurements of the branching fractions of $\eta_c \to K^+K^-\pi^0$, $K^0_S K^\pm \pi^\mp$, $2(\pi^+\pi^-\pi^0)$, and $p\bar{p}$, Phys. Rev. D **100**, 012003 (2019).
[96] Y. Jia, Which hadronic decay modes are good for eta(b) searching: Double J/psi or something else?, Phys. Rev. D **78**, 054003 (2008).
[97] J. L. Albacete, N. Armesto, J. G. Milhano, C. A. Salgado, and U. A. Wiedemann, Numerical analysis of the Balitsky-Kovchegov equation with running coupling: Dependence of the saturation scale on nuclear size and rapidity, Phys. Rev. D **71**, 014003 (2005).
[98] J. L. Albacete, N. Armesto, J. G. Milhano, C. A. Salgado, and U. A. Wiedemann, Nuclear size and rapidity dependence of the saturation scale from QCD evolution and experimental data, Eur. Phys. J. C **43**, 353 (2005).
[99] S. J. Brodsky, H. C. Pauli, and S. S. Pinsky, Quantum chromodynamics and other field theories on the light cone, Phys. Rep. **301**, 299 (1998).
[100] J. D. Bjorken, J. B. Kogut, and D. E. Soper, Quantum electrodynamics at infinite momentum: Scattering from an external field, Phys. Rev. D **3**, 1382 (1971).
[101] H. G. Dosch, T. Gousset, G. Kulzinger, and H. J. Pirner, Vector meson leptoproduction and nonperturbative gluon fluctuations in QCD, Phys. Rev. D **55**, 2602 (1997).
[102] V. Shtabovenko, R. Mertig, and F. Orellana, New developments in FeynCalc 9.0, Comput. Phys. Commun. **207**, 432 (2016).
[103] R. Mertig, M. Böhm, and A. Denner, Feyn Calc: Computer-algebraic calculation of Feynman amplitudes, Comput. Phys. Commun. **64**, 345 (1991).